nature cell biology

ARTICLES

https://doi.org/10.1038/s41556-018-0229-6

TBK1 and IKKε prevent TNF-induced cell death by RIPK1 phosphorylation

Elodie Lafont[1,6], Peter Draber[1,2,6], Eva Rieser[1,6], Matthias Reichert[1,6], Sebastian Kupka[1], Diego de Miguel[1], Helena Draberova[1,2], Anne von Mässenhausen[3], Amandeep Bhamra[4], Stephen Henderson[5], Katarzyna Wojdyla[4], Avigayil Chalk[2], Silvia Surinova[2,4], Andreas Linkermann[3] and Henning Walczak[1*]

The linear-ubiquitin chain assembly complex (LUBAC) modulates signalling via various immune receptors. In tumour necrosis factor (TNF) signalling, linear (also known as M1) ubiquitin enables full gene activation and prevents cell death. However, the mechanisms underlying cell death prevention remain ill-defined. Here, we show that LUBAC activity enables TBK1 and IKKε recruitment to and activation at the TNF receptor 1 signalling complex (TNFR1-SC). While exerting only limited effects on TNF-induced gene activation, TBK1 and IKKε are essential to prevent TNF-induced cell death. Mechanistically, TBK1 and IKKε phosphorylate the kinase RIPK1 in the TNFR1-SC, thereby preventing RIPK1-dependent cell death. This activity is essential in vivo, as it prevents TNF-induced lethal shock. Strikingly, NEMO (also known as IKKγ), which mostly, but not exclusively, binds the TNFR1-SC via M1 ubiquitin, mediates the recruitment of the adaptors TANK and NAP1 (also known as AZI2). TANK is constitutively associated with both TBK1 and IKKε, while NAP1 is associated with TBK1. We discovered a previously unrecognized cell death checkpoint that is mediated by TBK1 and IKKε, and uncovered an essential survival function for NEMO, whereby it enables the recruitment and activation of these non-canonical IKKs to prevent TNF-induced cell death.

TNFR1 signalling involves the formation of two distinct complexes[1]. The plasma membrane-associated TNFR1-SC, also termed complex-I, is responsible for gene activation, whereas the subsequently formed cytosolic complex-II induces cell death. Under physiological conditions, TNFR1 stimulation induces gene activation rather than cell death. However, aberrant TNF-induced signalling causes several autoimmune pathologies and cancer-related inflammation[2,3]. Therefore, defining the molecular checkpoints that determine the different TNFR1 signalling outputs is critical to understand the biology of inflammation.

Linear ubiquitylation is crucial for multiple immune receptor signalling pathways[4,5]. LUBAC is the only known E3 ligase capable of forming linear ubiquitin linkages. LUBAC is composed of the following three core proteins: haem-oxidized IRP2 ubiquitin ligase 1 (HOIL-1), SHANK-associated RH-domain-interacting protein (SHARPIN) and the catalytically active HOIL-1-interacting protein (HOIP)[6–9]. The essence of LUBAC and M1 ubiquitylation has been demonstrated by the embryonic lethality of mice lacking HOIL-1, HOIP or LUBAC activity[10–12], which is caused by aberrant TNFR1-mediated signalling[10,12].

LUBAC recruitment to complex-I enables full gene activation while preventing cell death[8,10,13,14]. Following the recruitment of LUBAC to the TNFR1-SC, several of its components, including RIPK1, NEMO, TNFR1 and TRADD, are M1 ubiquitylated by LUBAC[8,14,15]. In complex-I, M1 ubiquitin acts as a recruitment platform for adaptors such as NEMO, the regulatory subunit of the inhibitor of κB (IκB) kinase (IKK) complex. Although NEMO can be recruited to the TNFR1-SC in the absence of M1 ubiquitin, this process is much weaker than in its presence[13]. Accordingly, the binding of NEMO to the TNFR1-SC with M1 ubiquitin enables full activation of the canonical IKKs IKKα and IKKβ[16]. When activated, they phosphorylate IκB, causing the nuclear translocation of nuclear factor-κB (NF-κB), thereby initiating gene transcription. Independently, IKKα and IKKβ prevent TNF-induced cell death by phosphorylating RIPK1. This limits the ability of RIPK1 to promote the formation of complex-II[17]. Phosphorylation events on RIPK1, mediated by the p38 target MK2, also restrict the capacity of RIPK1 to trigger complex-II formation and, consequently, cell death[18–20]. Notably, IKKα, IKKβ and p38 and MK2 also mediate gene expression downstream of TAK1, which is required for TNF-induced gene activation[16,21–26].

TBK1 and IKKε are two closely related kinases that are homologous to the canonical kinases IKKα and IKKβ[27,28]. Various adaptors recruit TBK1 and IKKε to distinct immune signalling complexes[29]. Concomitant TBK1 and IKKε ablation abolishes the activation of interferon signalling by various immune receptors, including TLR3 and TLR4, or after viral infection[30,31]. Here, we show that by phosphorylating RIPK1 in complex-I, TBK1 and IKKε serve an essential function in TNF signalling, providing a physiologically relevant cell death-restricting checkpoint that depends on M1 ubiquitylation and NEMO.

Results

Effective TBK1 and IKKε recruitment to and activation in complex-I require LUBAC activity. To elucidate how LUBAC modulates TNF signalling, we compared the composition of purified TNFR1-SCs from wild-type and HOIP-deficient A549 cells by mass spectrometry (MS)[14]. This confirmed that in

[1]Centre for Cell Death, Cancer and Inflammation (CCCI), UCL Cancer Institute, University College London, London, UK. [2]Laboratory of Adaptive Immunity, Institute of Molecular Genetics of the Czech Academy of Sciences, Prague, Czech Republic. [3]Division of Nephrology, Department of Internal Medicine III, University Hospital Carl Gustav Carus at the Technical University Dresden, Dresden, Germany. [4]Proteomics Research Core Facility, UCL Cancer Institute, University College London, London, UK. [5]Bill Lyons Informatics Centre (BLIC), UCL Cancer Institute, University College London, London, UK. [6]These authors contributed equally: Elodie Lafont, Peter Draber, Eva Rieser, Matthias Reichert. *e-mail: h.walczak@ucl.ac.uk

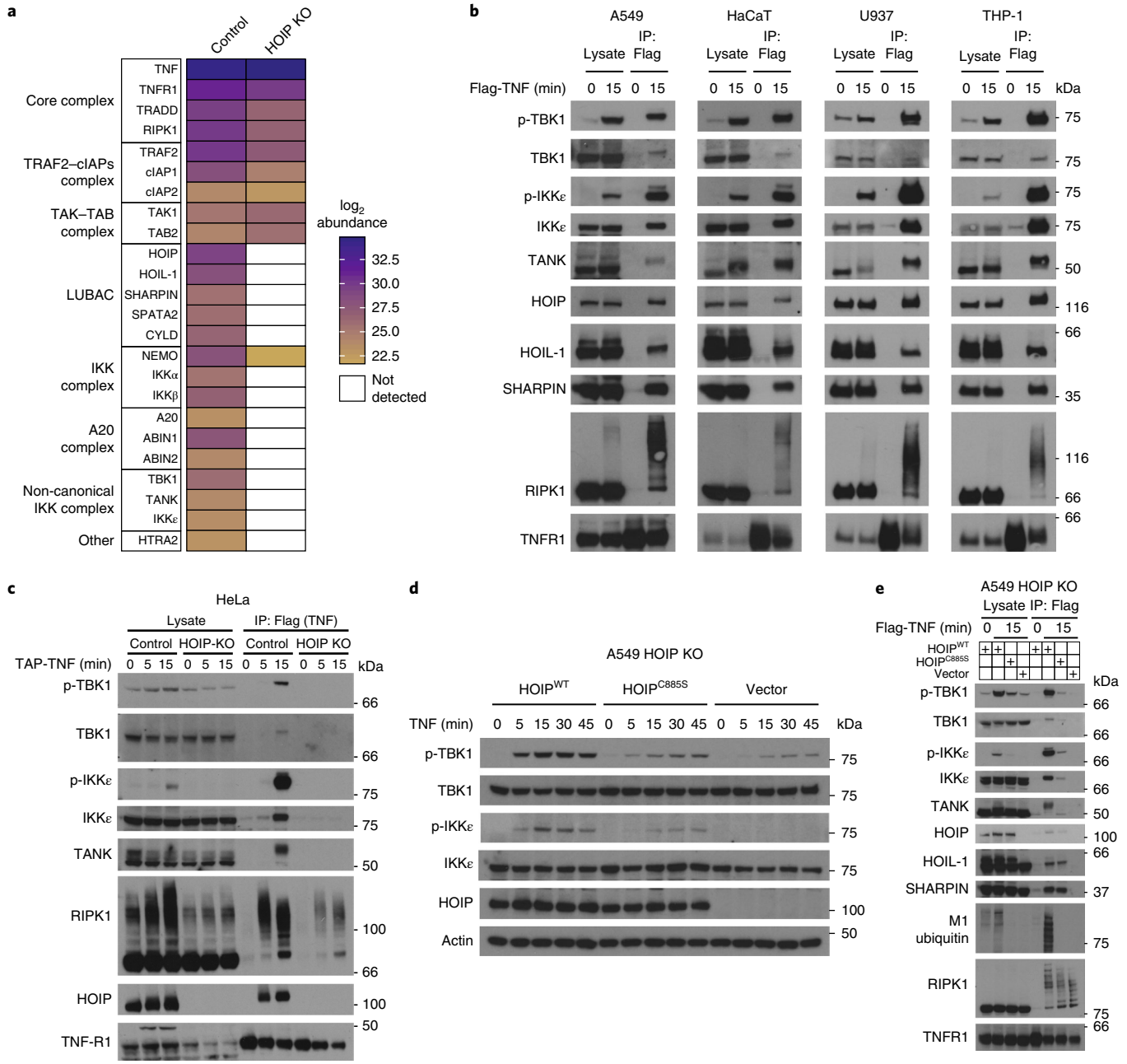

Fig. 1 | LUBAC mediates the recruitment and activation of the non-canonical kinases TBK1 and IKKε in the TNFR1-SC. a, A549 HOIP control or HOIP-deficient (HOIP KO) cells were stimulated with TAP-TNF (500 ng ml^{-1}) for 15 min. TNFR1-SC was purified in a two-step immunoprecipitation process via TAP-Tag and analysed by LC–MS/MS. The mean protein abundance for two independent experiments and two LC–MS analyses is plotted as indicated. Raw data can be accessed at the ProteomeXchange Consortium via the PRIDE[70] partner repository with the dataset identifier PXD008497; analysed data are provided in Supplementary Table 2. **b**, A549, HaCaT, U937 and THP-1 cells were stimulated with FLAG-TNF (1 μg ml^{-1}) for the indicated times. TNFR1-SC was purified and analysed by western blotting. **c**, HeLa HOIP control or HOIP-deficient cells were stimulated with TAP-TNF (500 ng ml^{-1}) and subjected to TNFR1-SC isolation and western blot analysis. **d**, HOIP-deficient A549 cells were reconstituted with empty vector, HOIP^{WT} or enzymatically inactive HOIP^{C885S} and were stimulated with TNF (200 ng ml^{-1}) for the indicated times, and lysates were analysed by western blotting. **e**, HOIP-deficient A549 cells reconstituted with empty vector, HOIP^{WT} or enzymatically inactive HOIP^{C885S} were stimulated with FLAG-TNF (1 μg ml^{-1}) for the indicated time. Lysates and TNFR1-SC were analysed by western blotting. For **b**–**e**, one representative experiment out of two is shown. Unprocessed original scans of blots are shown in Supplementary Fig. 7.

HOIP-deficient cells, HOIL-1, SHARPIN, CYLD and SPATA2[14,32], as well as the A20–ABIN1–ABIN2 complex, are missing from complex-I, whereas NEMO is still recruited to it, albeit poorly[14,16,2532–36] (Fig. 1a; Supplementary Table 2). Importantly, however, TBK1, IKKε and one of their known adaptors, TANK[37], were detected in complex-I in control but not HOIP-deficient cells (Fig. 1a).

A western blot analysis revealed that TBK1 and IKKε are recruited to and strongly phosphorylated within the native TNFR1-SC on the activatory S172 residue[38] in various HOIP-proficient cell lines, whereas their activation in corresponding HOIP-deficient cells is very weak (Fig. 1b,c; Supplementary Fig. 1a,b). Thus, TBK1 and IKKε are bona fide components of complex-I, and LUBAC enables their recruitment.

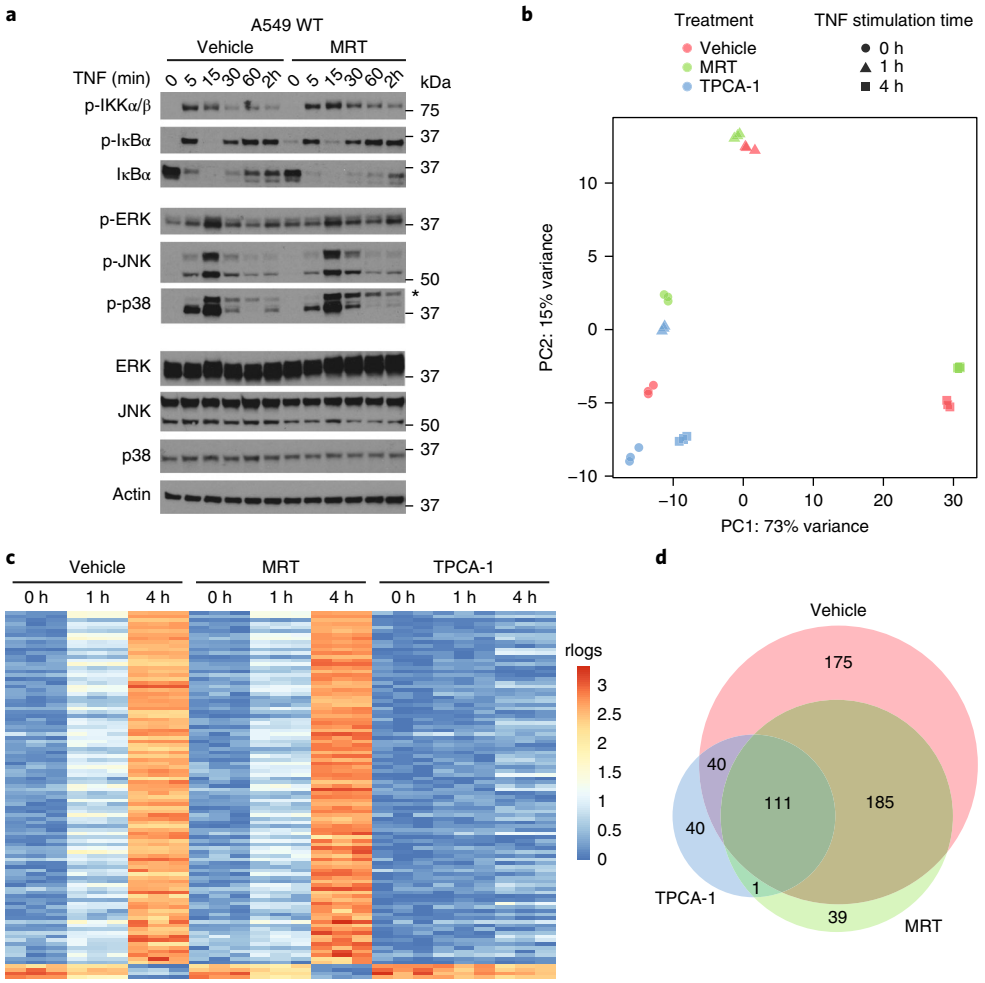

Fig. 2 | Inhibition of TBK1 and IKKε exerts only minor effects on TNF-induced gene activatory signalling. a–d, A549 wild-type (WT) cells were pre-incubated with either vehicle (DMSO) or MRT for 30 min, followed by stimulation with TNF (200 ng ml^{-1}) for the indicated times. **a**, Lysates were analysed by western blotting. One representative experiment out of two is shown. The asterisk indicates staining from previous p-JNK. Unprocessed original scans of blots are shown in Supplementary Fig. 7. **b–d**, Cells were lysed, their total RNA extracted and RNA-seq analysis performed. Samples from three independent experiments were obtained and analysed. A principal component (PC) analysis of A549 samples based on transcriptome-wide expression level data is shown (**b**). The heatmap (**c**) illustrates the major change of expression across the dataset. The genes shown are the 100 that were most highly correlated with PC1 (see **b**). To increase the clarity of the comparison, the rlog (regularised logs to normalise read counts) expression data of each row were zeroed at time point 0 h and then scaled by the standard deviation. The RNA-seq raw dataset for **b** and **c** are available in the SRA repository and can be accessed using the BioProject accession number PRJNA422567 or SRA accession number SRP126844 (https://www.ncbi.nlm.nih.gov/Traces/study/?acc=SRP126844). The Venn diagram (**d**) represents the number of all transcripts significantly regulated following 1 h of TNF stimulation in samples treated with vehicle, MRT or TPCA-1 and the transcript overlap between these three groups. Corresponding transcripts can be found in Supplementary Table 3. Differential RNA-seq expression statistics (*P* values) on contrasting biological triplicates, corresponding to samples obtained from three independent experiments (groups as in **b–d**), were estimated using DESeq2. Adjusted *P* value statistics were calculated using the Benjamini–Hochberg and IHW adjustment.

Using HOIP-deficient HeLa and A549 cells reconstituted with wild-type HOIP (HOIP^{WT}) or catalytically inactive HOIP (HOIP^{C885S})[39], we determined that effective TBK1 and IKKε recruitment to complex-I requires the M1 ubiquitin-forming activity of LUBAC, as TBK1 and IKKε recruitment was strongly diminished in HOIP-deficient HeLa and A549 cells whether or not HOIP^{C885S} was re-expressed in them (Fig. 1d,e; Supplementary Fig. 1c,d).

The role of TBK1 and IKKε in TNF-induced gene activation is limited. As TBK1 and IKKε are crucial for gene expression by various immune receptor complexes[30,40–42], we evaluated whether these kinases influenced TNF-induced gene activation by generating L929 cells in which TBK1, IKKε and TNF are all knocked out. The absence of TBK1 and IKKε did not significantly affect TNF-induced gene activatory signalling and, if anything, slightly increased IκBα phosphorylation (Supplementary Fig. 2a). This result is in line with the previously proposed roles of TBK1 and IKKε as negative regulators of IKKα and IKKβ activation[43]. Similarly, in mouse embryonic fibroblasts (MEFs) and A549 cells, treatment with the TBK1 and IKKε-specific inhibitor MRT67307[43] (MRT) did not exert any significant effects on the TNF-induced activation of MAPKs or NF-κB (Fig. 2a; Supplementary Fig. 2b). Next, we evaluated whether TBK1 and IKKε affect gene induction following TNFR1 stimulation. We performed an unbiased RNA sequencing (RNA-seq) analysis following TNF versus TNF plus MRT stimulation, also including TNF and TPCA-1, which, as an IKKα and IKKβ-inhibiting control, is known to profoundly affect TNF-induced gene expression[44].

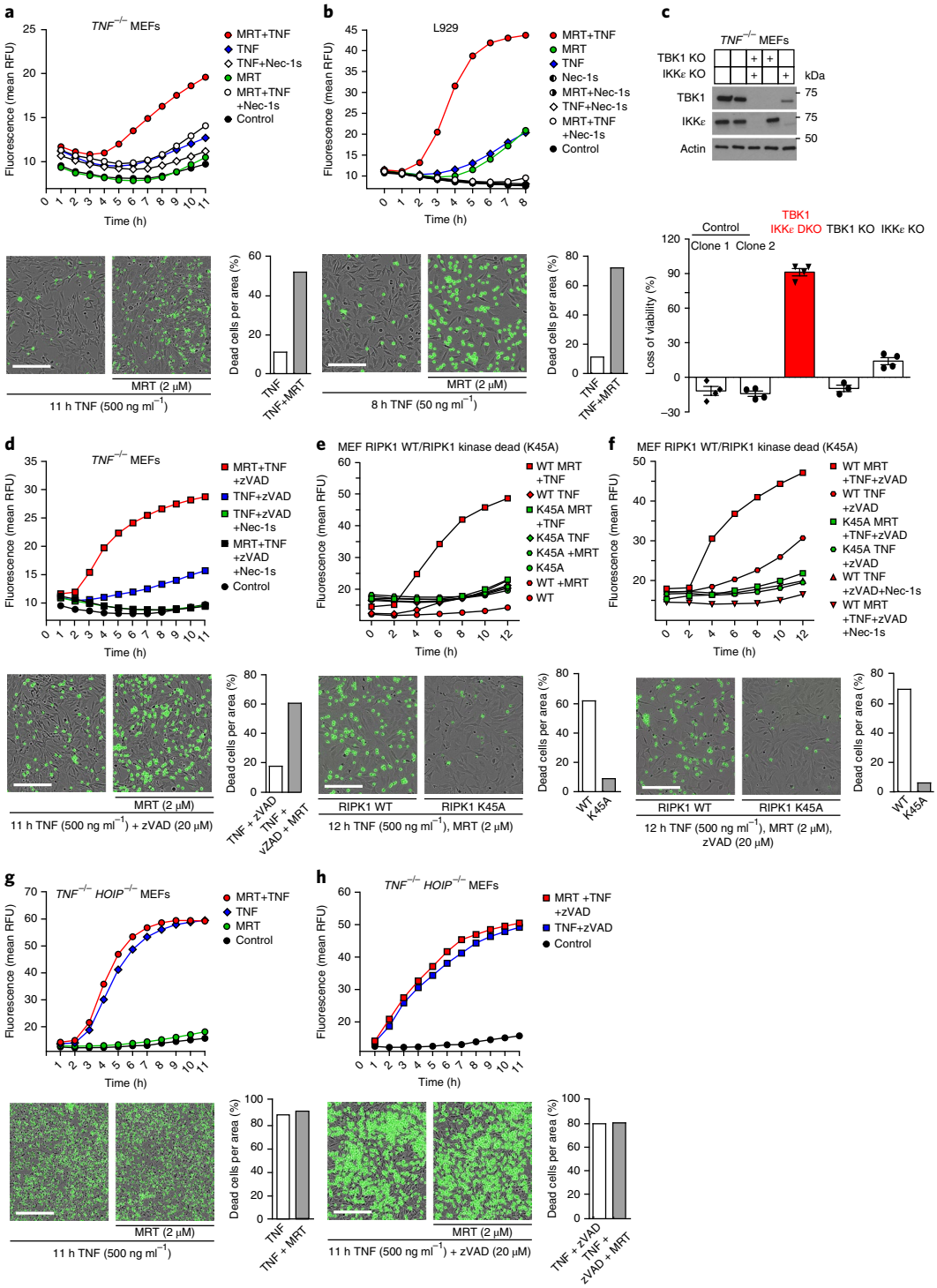

Fig. 3 | Inhibition of TBK1 and IKKε sensitizes cells to TNF-induced RIPK1-dependent cell death downstream of LUBAC. a,**b**, *TNF*$^{-/-}$ MEFs (**a**) and L929 cells (**b**) were treated with TNF (500 ng ml^{-1} and 50 ng ml^{-1}, respectively) in the presence or absence of MRT and Nec-1s. **c**, *TNF*$^{-/-}$ MEFs of the indicated genotype were stimulated with TNF (500 ng ml^{-1}) for 6 h. Loss of cell viability was determined using the CellTiter-Glo assay. Mean ± s.e.m. of $n = 3$ independent experiments. Lysates of untreated cells were analysed by western blotting. Unprocessed original scans of blots are shown in Supplementary Fig. 7. **d**–**h**, MEFs of the indicated genotype were treated with TNF (500 ng ml^{-1}) in the presence or absence of the indicated compounds. For **a**, **b** and **d**–**h**, cell death was measured as a function of time by Sytox Green positivity. The RFU mean of four technical replicates of one representative experiment out of three independent experiments is represented. Representative images of indicated measurements are depicted with the corresponding percentage of dead cells. Cell counting was performed manually using ImageJ. Scale bars, 200 μm. Raw data are provided in Supplementary Table 1.

A principal component analysis revealed that TNF drastically modulated gene expression, with TNF-treated cells clearly segregated from untreated samples. While the effect of IKKα and IKKβ inhibition on TNF-induced gene expression was substantial, the effect of TBK1 and IKKε inhibition was surprisingly limited (Fig. 2b). The top 100 most altered transcripts were highly similar

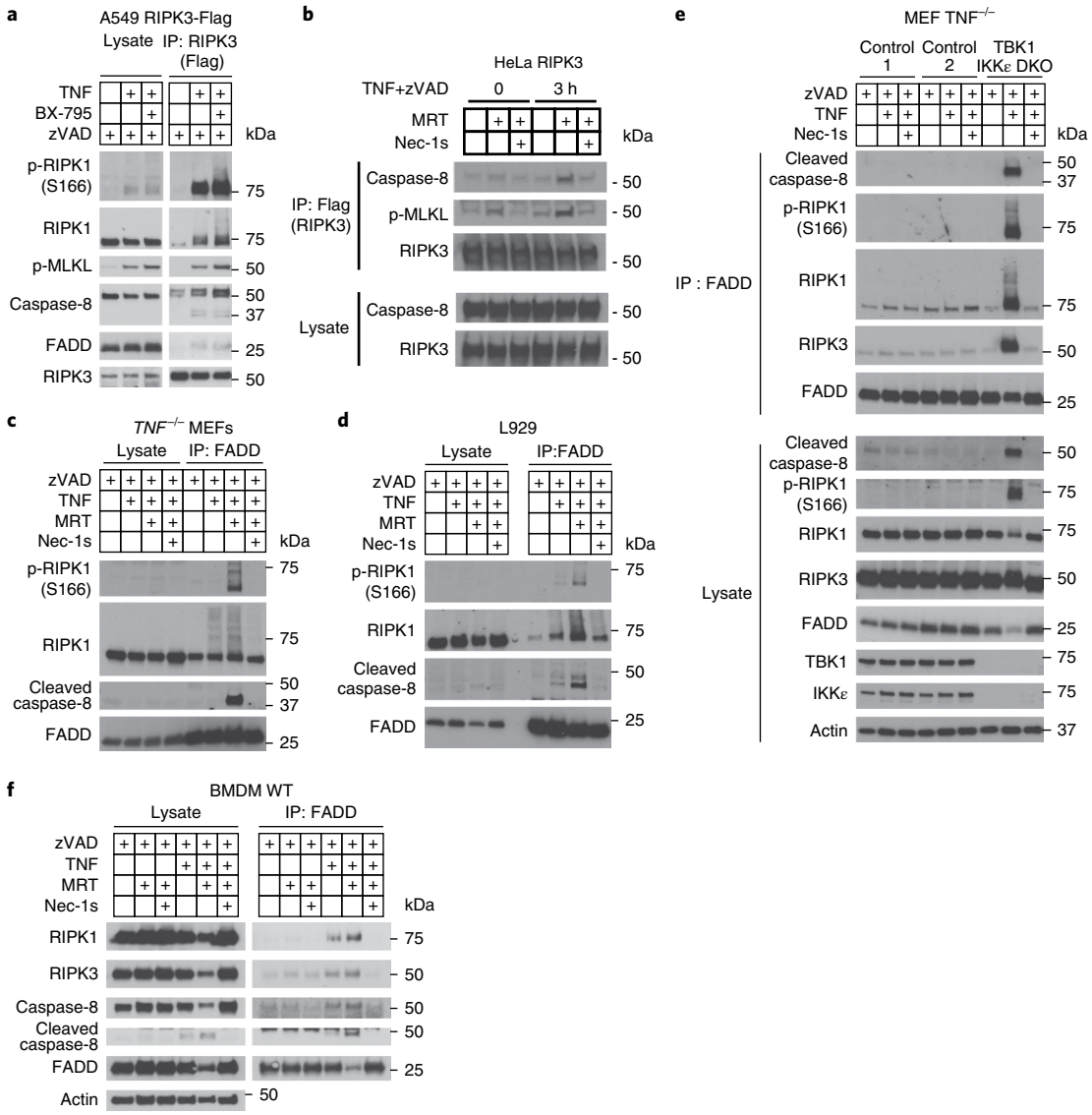

Fig. 4 | Inhibition of TBK1 and IKKε leads to TNF-induced RIPK1 activation and increased complex-II formation. a,**b**, A549 (**a**) and HeLa (**b**) cells both overexpressing FLAG-tagged RIPK3 were treated with or without BX-795 and zVAD-FMK (**a**) or MRT, zVAD-FMK and Nec-1s (**b**) and were stimulated with TNF (500 ng ml^{-1}) for 3 h. Complex-II was then FLAG-immunoprecipitated and analysed by western blotting. **c–f**, *TNF*$^{-/-}$MEFs (**c**), L929 cells (**d**), *TNF*$^{-/-}$ MEFs with TBK1 and IKKε knocked out (DKO) and corresponding *TNF*$^{-/-}$ MEF control cells (**e**), and primary BMDMs (**f**) were pretreated with MRT in combination with zVAD-FMK and Nec-1s as indicated and stimulated with TNF (500 ng ml^{-1}) for either 6 h (**c**, **e**, **f**) or 4 h (**d**). Complex-II was then immunoprecipitated with a FADD antibody and analysed by western blotting. For all panels, one representative experiment is shown out of two independent experiments. Unprocessed original scans of blots are shown in Supplementary Fig. 7.

between TNF-stimulated control cells and TNF and MRT-treated cells, but significantly different in TNF and TPCA-1-treated cells (Fig. 2c; Supplementary Fig. 2c). Notably, the majority of transcripts with significantly altered expression at the 1-h time point in control cells were similarly modulated in TNF and MRT-treated cells but not in TNF and TPCA-1-treated cells (Fig. 2d; Supplementary Table 3). Thus, in contrast to the roles of TBK1 and IKKε as drivers of gene induction in other immune signalling pathways[40,41], their role in TNF-induced gene expression is limited.

TBK1 and IKKε prevent TNF-induced RIPK1-dependent cell death. We next assessed the role of TBK1 and IKKε in TNF-induced cell death. Strikingly, treatment with MRT or another TBK1 and IKKε-specific inhibitor, BX-795[45], drastically sensitized MEFs and L929 cells to TNF-induced death (Fig. 3a,b; Supplementary Fig. 3a). Intriguingly, in both cases, cell death was prevented by the RIPK1 inhibitor Nec-1s (Fig. 3a,b; Supplementary Fig. 3a). Interestingly, the MRT-induced spontaneous death of L929 cells was inhibited by the TNF blocker etanercept (also known as Enbrel; Supplementary Fig. 3b). Next, we created TNF-deficient MEFs and L929 cells in which we further deleted TBK1, IKKε or both kinases to enable us to genetically assess their cell death-preventive function. In line with the results obtained when these kinases were inhibited, concomitant deletion of TBK1 and IKKε strongly sensitized these cells to TNF-induced death (Fig. 3c; Supplementary Fig. 3c,d). Thus, both pharmacological inhibition and genetic ablation of TBK1 and IKKε sensitizes cells to TNF-induced death.

We next investigated the cell death modality induced by TBK1 and IKKε inhibition. While pretreatment with the pan-caspase inhibitor zVAD-FMK (carbobenzoxy-valyl-alanyl-aspartyl-[O-methyl]-fluoromethylketone) substantially sensitized MEFs to TNF alone, sensitization to TNF and MRT was significantly higher

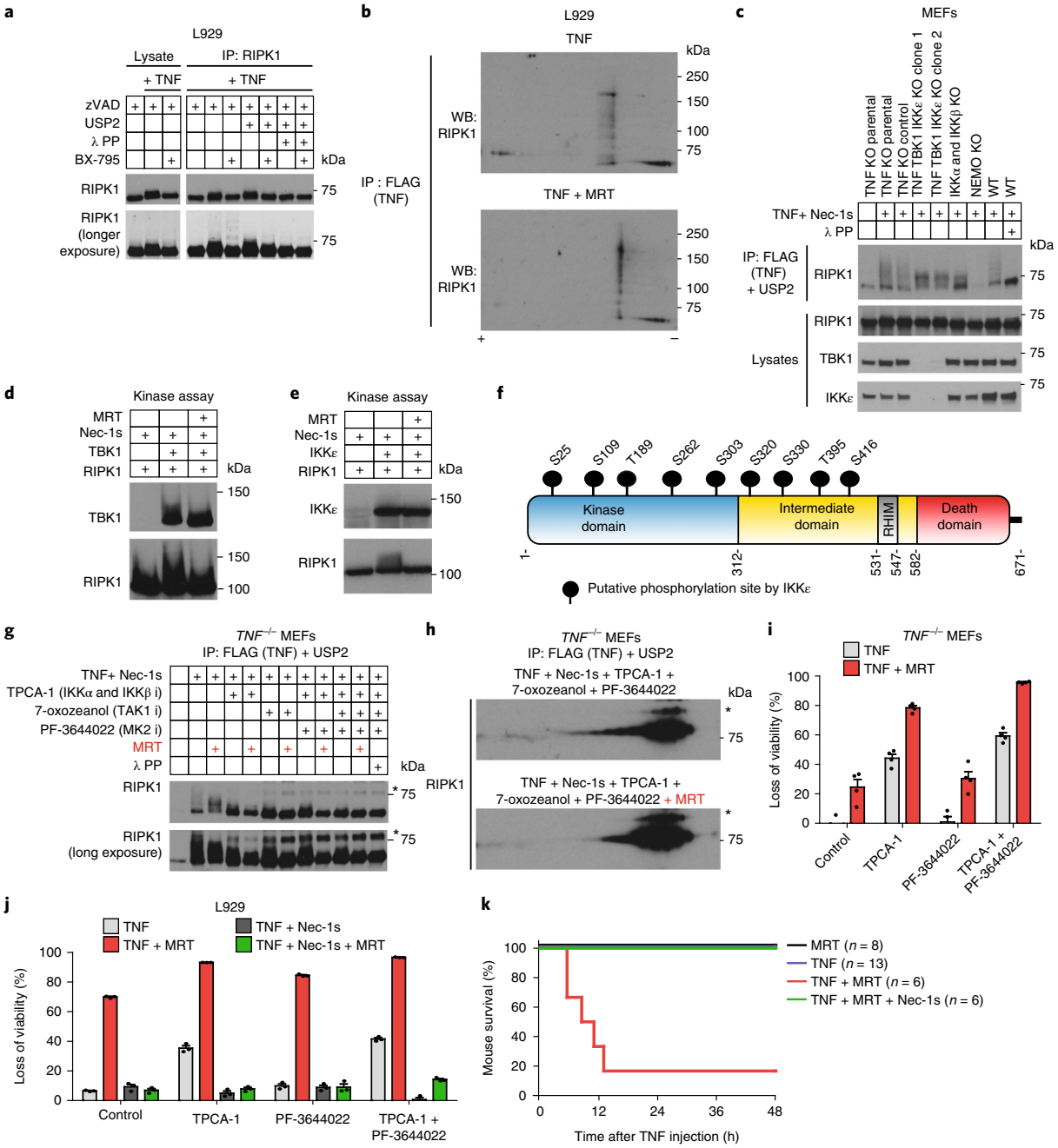

Fig. 5 | TBK1 and IKKε phosphorylate RIPK1 both in vitro and at the TNFR1-SC, providing a physiologically relevant cell death checkpoint. a, L929 cells pretreated with or without BX-795 were stimulated with TNF (1 μg ml^{-1}) and zVAD-FMK for 15 min before RIPK1 pull down. RIPK1 immunoprecipitate (IP) treated with USP2 and λ-phosphatase (λ PP) as indicated was analysed by western blotting. **b**, L929 cells were stimulated with TAP-TNF for 15 min (1 μg ml^{-1}) with or without MRT. TNFR1-SC was FLAG-immunoprecipitated. Samples were first separated by pI on IPG strips pH 3–10 NL, followed by SDS–PAGE and western blot analysis. **c**, Indicated MEFs were treated with FLAG-TNF (1 μg ml^{-1}) and Nec-1s, followed by FLAG-IP. TNFR1-SC treated with USP2 and λ-phosphatase as indicated was analysed by western blotting. **d**,**e**, GST-tagged TBK1 (**d**) and IKKε (**e**) were incubated with GST-tagged RIPK1 in a kinase assay with or without the indicated inhibitors before western blot analysis. **f**, Phosphosites identified by LC–MS/MS from one kinase assay using GST-tagged RIPK1, Nec-1s and IKKε. RHIM, RIP homotypic interaction motif. Raw data are accessible at the ProteomeXchange Consortium via the PRIDE[70] partner repository with the dataset identifier PXD008518; analysed data are provided in Supplementary Table 4. **g**, *TNF*$^{-/-}$ MEFs pretreated with indicated inhibitors (i) were stimulated with FLAG-TNF (1 μg ml^{-1}) and Nec-1s for 15 min, followed by FLAG-IP. TNFR1-SCs treated with USP2 and λ-phosphatase as indicated were analysed via western blotting. The asterisks indicate nonspecific bands. **h**, *TNF*$^{-/-}$ MEFs pretreated with indicated inhibitors were stimulated with FLAG-TNF (1 μg ml^{-1}) and Nec-1s for 15 min, followed by FLAG-IP. TNFR1-SCs treated with USP2 were first separated by pI on IPG strips pH 4–7 followed by SDS–PAGE and western blot analysis. **i**, *TNF*$^{-/-}$ MEFs stimulated with indicated inhibitors for 30 min were treated with TNF (500 ng ml^{-1}) for 7 h. **j**, L929 pre-incubated with Nec-1s for 15 min and further incubated with indicated inhibitors for 30 min were treated with TNF (50 ng ml^{-1}) for 4 h. **i**,**j**, Loss of cell viability was determined by CTG assay. Mean ± s.e.m. of $n = 4$ (**i**) or mean ± s.e.m. of $n = 3$ (**j**) independent experiments. **k**, Cumulative survival rates of mice following TNF-α-induced shock in the presence of indicated inhibitors were compared using log-rank Mantel–Cox tests. MRT versus TNF + MRT, $P < 0.001$; TNF versus TNF + MRT, $P < 0.0001$; TNF + MRT versus TNF + MRT + Nec-1s, $P = 0.0061$. Unprocessed blots are shown in Supplementary Fig. 7, raw data in Supplementary Table 1. One experiment representative of two (**a**–**c**, **g**, **h**) or three (**d**, **e**) independent experiments is shown.

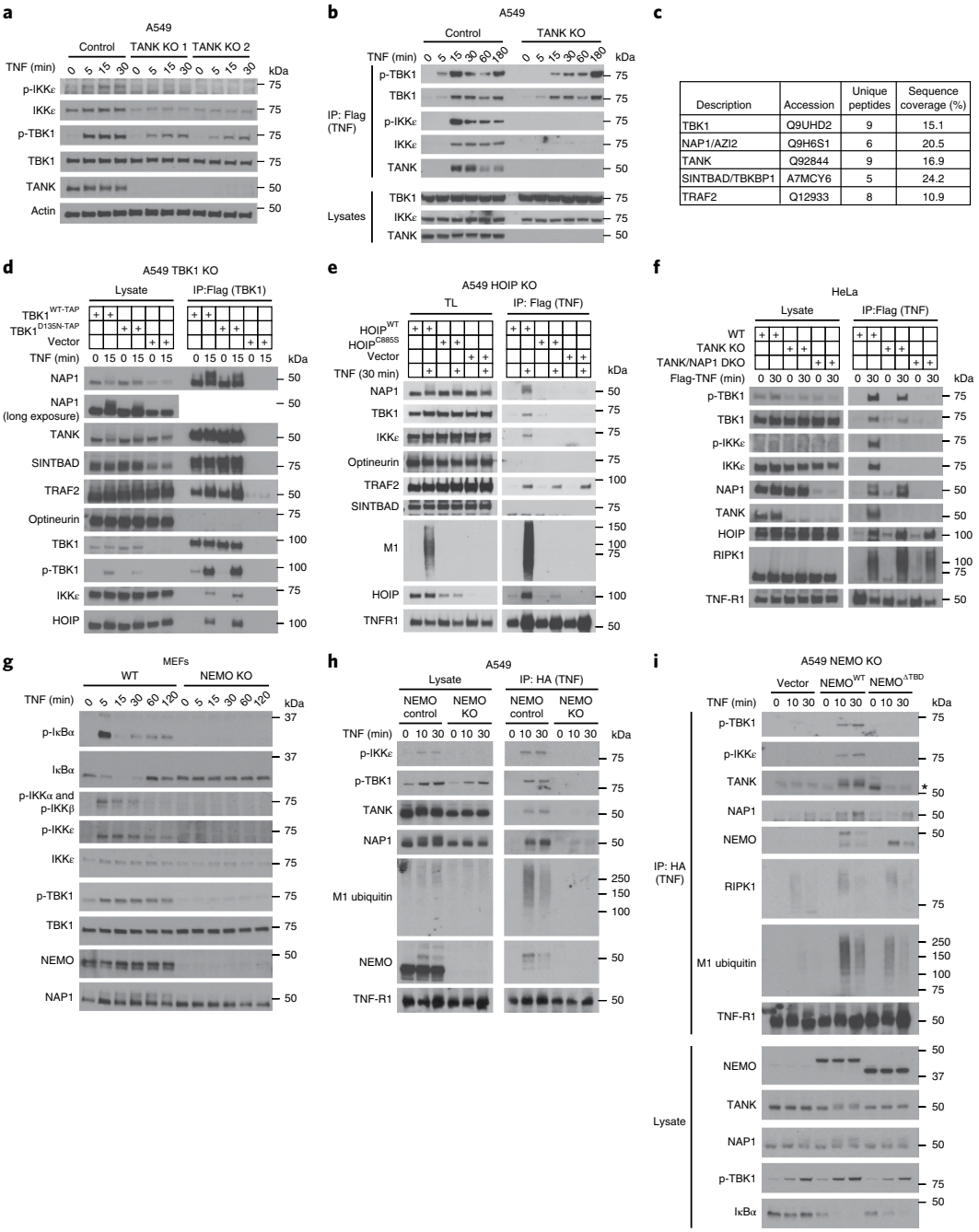

Fig. 6 | NEMO acts upstream of the adaptors TANK and NAP1, which recruit TBK1 and IKKε, or TBK1 only, respectively, to the TNFR1-SC. a, TANK-deficient A549 cell clones and control cells were treated with TNF (200 ng ml^{-1}) for the indicated times. Lysates were analysed by western blotting. **b**, TANK-deficient or corresponding control A549 cells were stimulated with FLAG-TNF (500 ng ml^{-1}) for the indicated times. The purified TNFR1-SC and lysates were analysed by western blotting. **c**, A549 TBK1-deficient cells were reconstituted with TBK1$^{WT\text{-}TAP}$. The TBK1 interactome was purified in a two-step immunoprecipitation process via TAP-tag and analysed by LC–MS/MS. One experiment was analysed. Raw data can be accessed at the ProteomeXchange Consortium via the PRIDE[70] partner repository with the dataset identifier PXD010777; analysed data are provided in Supplementary Table 5. **d**, A549 TBK1-deficient cells were reconstituted with TBK1$^{WT\text{-}TAP}$ or the catalytically inactive mutant TBK1$^{D135N\text{-}TAP}$ and treated with TNF (500 ng ml^{-1}) as indicated. The purified TBK1-associated complex and lysates were analysed by western blotting. **e**, HOIP-deficient A549 cells reconstituted with HOIP^{WT}, enzymatically inactive HOIP^{C885S} or vector control were stimulated with FLAG-TNF (500 ng ml^{-1}) for the indicated times. The purified TNFR1-SC and lysates were analysed by western blotting. **f**, HeLa TANK-deficient cells, concomitantly deficient in TANK and NAP1 (TANK/NAP1 DKO), or corresponding control cells were stimulated with TAP-TNF (500 ng ml^{-1}) and subjected to immunoprecipitation via Flag. The purified TNFR1-SC and lysates were analysed by western blotting. **g**, NEMO-deficient and corresponding wild-type MEFs were stimulated with TNF (200 ng ml^{-1}) for the indicated times. Lysates were analysed by western blotting. **h**, A549 control and NEMO-deficient cells were stimulated with HA-TNF (1 μg ml^{-1}) and subjected to immunoprecipitation via HA. The purified TNFR1-SC and lysates were analysed by western blotting. **i**, A549 NEMO-deficient cells reconstituted with NEMO^{WT}, NEMO$^{\Delta TBD}$ or vector control were stimulated with HA-TNF (1 μg ml^{-1}) for the indicated times. The purified TNFR1-SC and lysates were analysed by western blotting. One experiment representative of two (**a**, **b**, **d**–**g**) or three independent experiments (**h**, **i**) is shown. Unprocessed original scans of blots are shown in Supplementary Fig. 7.

(Fig. 3d; Supplementary Fig. 3e). Importantly, RIPK1 kinase-dead MEFs were resistant to MRT-induced death sensitization by TNF or TNF plus zVAD-FMK (Fig. 3e,f). In line with the finding that LUBAC is required for effective TNF-induced TBK1 and IKKε activation, inhibition of both TBK1 and IKKε did not sensitize HOIP-deficient MEFs to TNF-induced or zVAD-FMK plus TNF-induced cell death (Fig. 3g,h). Moreover, MRT-mediated sensitization to TNF-induced necroptosis occurred in human A549 cells expressing RIPK3 (Supplementary Fig. 3f–h). Notably, MEFs were also sensitized to TNF-induced death in the presence of cycloheximide, indicating that protein synthesis is not necessary for the sensitization mediated by TBK1 and IKKε inhibition (Supplementary Fig. 3i,j). MRT also sensitized primary bone marrow-derived macrophages (BMDMs) to TNF-induced RIPK1-dependent death (Supplementary Fig. 4a). Again, a substantial percentage of MRT-only-treated BMDMs were killed by endogenous TNF (Supplementary Fig. 4b). Interestingly, BMDMs were exclusively sensitized to TNF-induced apoptosis (Supplementary Fig. 4c). Accordingly, the absence of the necroptosis-mediating pseudokinase MLKL did not diminish TNF and MRT-induced BMDM death, while the ablation of both caspase-8 and MLKL abrogated it (Supplementary Fig. 4d,e).

Together, these results demonstrate that the inhibition or absence of TBK1 and IKKε promotes TNF-induced apoptosis and/or necroptosis, which depends on the ability of a given cell type to undergo death by the respective modality. Importantly, in either case, cell death induction requires the activity of RIPK1.

TBK1 and IKKε prevent TNF-induced RIPK1 activation and ensuing complex-II formation. TNFR1-SC assembly precedes the formation of complex-II, which contains RIPK1, FADD, FLIP, caspase-8, RIPK3 and MLKL. Depending on the cellular context and the relative expression of pro- and anti-apoptotic and pro- and anti-necroptotic proteins[15,46–48], complex-II can trigger apoptosis or necroptosis. RIPK1 kinase activity mediates complex-II formation and is therefore generally required for TNF-induced cell death[17].

Since the kinase activity of RIPK1 is required for TNF-induced cell death when TBK1 and IKKε are absent or inhibited, we assessed whether TBK1 and IKKε prevent cytotoxicity by preventing RIPK1 from mediating complex-II formation. We treated A549 cells expressing TAP (tandem affinity purification)-tagged RIPK3 with TNF and zVAD-FMK or a combination of TNF, zVAD-FMK and BX-795 before immunoprecipitating RIPK3. TBK1 and IKKε inhibition markedly enhanced the association of RIPK3 with caspase-8 and FADD, phosphorylated MLKL (p-MLKL) and phosphorylated RIPK1 (p-RIPK1) (Fig. 4a). Enhanced RIPK3 binding to caspase-8 and p-MLKL was also observed in RIPK3-expressing HeLa cells and, decisively, concomitant RIPK1 inhibition prevented complex-II formation (Fig. 4b).

In accordance with the increased cell death observed following TBK1 and IKKε inhibition, L929 cells and MEFs also displayed increased RIPK1 activation and complex-II formation following TNF, zVAD-FMK and MRT co-treatment (Fig. 4c,d). Importantly, genetic TBK1 and IKKε co-ablation in MEFs (Fig. 4e) and TNF and MRT treatment of primary BMDMs (Fig. 4f) also substantially enhanced complex-II formation. In all cases, complex-II formation was dependent on RIPK1 kinase activity (Fig. 4b-f). Hence, TBK1 and IKKε prevent TNF-induced cell death by restricting RIPK1 autoactivation and consequent complex-II formation.

TBK1 and IKKε mediate phosphorylation of RIPK1 in the TNFR1-SC. We hypothesized that the negative effect of TBK1 and IKKε on RIPK1 autophosphorylation might be achieved via TNF-induced RIPK1 phosphorylation mediated by these kinases. Thus, we determined whether we could detect any TBK1- and IKKε-dependent phosphorylation of RIPK1. After immunoprecipitating RIPK1 from L929 cells treated with TNF or TNF and BX-795 in the presence of zVAD-FMK, we incubated the resulting immunoprecipitates with or, as a control, without the pan-deubiquitinase USP2 to completely deubiquitylate RIPK1. This was done with or without λ-phosphatase to uncover any RIPK1 phosphorylation that requires TBK1 and IKKε activity (Fig. 5a). USP2 treatment resulted in the collapse of most modified high-molecular-weight forms onto low-molecular-weight forms of RIPK1. The intermediate-molecular-weight forms remaining after USP2 treatment completely collapsed onto the band of unmodified RIPK1 following treatment with λ-phosphatase. This result demonstrates that phosphorylation accounts for the TBK1 and IKKε-dependent mobility shift of deubiquitylated RIPK1. Interestingly, TNF and BX-795 co-treatment reduced the RIPK1 mobility shift compared to TNF treatment. Most importantly, this shift was not seen following λ-phosphatase treatment, demonstrating that TBK1 and IKKε inhibition specifically prevents RIPK1 phosphorylation (Fig. 5a).

To assess whether TBK1- and IKKε-dependent RIPK1 phosphorylation occurs in the TNFR1-SC, we immunoprecipitated complex-I following TNF versus TNF and MRT treatment before evaluating the status of RIPK1 phosphorylation by two-dimensional (2D) gel electrophoresis. This revealed that TBK1 and IKKε inhibition reduced the low isoelectric point (pI) forms of RIPK1 after TNF stimulation in complex-I (Fig. 5b). Importantly, RIPK1 phosphorylation in complex-I was also reduced in MEFs and L929 cells in which TNF, TBK1 and IKKε were knocked out, and in MEFs in which TNF and TBK1 were knocked out (Fig. 5c; Supplementary Fig. 5a). We therefore conclude that TBK1 and IKKε promote RIPK1 phosphorylation within the native TNFR1-SC.

Performing in vitro kinase assays to test whether TBK1 and IKKε can directly phosphorylate RIPK1 revealed that both kinases were able to do so (Fig. 5d,e). A MS analysis of the in vitro kinase assay employing recombinant IKKε and RIPK1 in the presence of Nec-1s showed that RIPK1 was phosphorylated on numerous residues, as also confirmed by 2D gel electrophoresis (Fig. 5f; Supplementary Fig. 5b; Supplementary Table 4). Notably, several of these residues have been reported to be phosphorylated by other kinases[17–20].

Together, these results show that TBK1 and IKKε mediate RIPK1 phosphorylation on multiple residues in complex-I, thereby preventing RIPK1 autophosphorylation and the consequent formation of complex-II.

TBK1 and IKKε phosphorylate RIPK1 independently from IKKα, IKKβ and MK2. TNF-induced RIPK1 activation is controlled by phosphorylation that is mediated by IKKα, IKKβ and MK2, all acting downstream of TAK1[17–20]. These phosphorylation events function as checkpoints to inhibit RIPK1-dependent complex-II formation. We next determined whether the TBK1- and IKKε-mediated RIPK1 phosphorylation represents a distinct cell death-preventing checkpoint. We purified the TNFR1-SC from cells treated with TNF together with different inhibitors or combinations thereof targeting TBK1 and IKKε (MRT), IKKα and IKKβ (TPCA-1), MK2 (PF-3644022) and TAK1 (7-oxozeanol) before treating the immunoprecipitated complexes with USP2 to visualize phosphorylation events. This analysis confirmed that inhibition of TAK1, MK2 and/or IKKα and IKKβ reduces RIPK1 phosphorylation in complex-I. Importantly, however, TBK1 and IKKε phosphorylated RIPK1 independently of MK2 and of IKKα and IKKβ, as only the combined inhibition of TBK1 and IKKε, either with that of TAK1 or with those of MK2 and IKKα and IKKβ, abrogated RIPK1 phosphorylation (Fig. 5g).

A 2D gel analysis of complex-I further revealed that several low-pI forms of RIPK1 disappeared after the addition of MRT in conditions under which all other known phosphorylation events are inhibited (Fig. 5h). Thus, TBK1 and IKKε activity in complex-I promotes the phosphorylation of RIPK1 at multiple sites that are not phosphorylated by other RIPK1-inhibiting kinases. In line with

a distinct checkpoint mediated by TBK1 and IKKε, their inhibition sensitized MEFs and L929 cells to RIPK1-dependent TNF-induced death even in the presence of MK2 and/or IKKα and IKKβ inhibitors (Fig. 5i,j). Thus, TBK1 and IKKε-mediated RIPK1 phosphorylation constitutes a cell death checkpoint that is different from previously described ones. Furthermore, these results strongly suggest that TBK1 and IKKε directly phosphorylate RIPK1 in the TNFR1-SC.

TBK1 and IKKε protect against TNF-induced RIPK1-dependent lethal shock in vivo. To reveal whether the cell death checkpoint identified herein is functionally relevant in vivo, we employed TNF at an established sublethal dose[17,20] in a murine model of TNF-induced shock that requires RIPK1-dependent cell death[49,50]. As expected, none of the mice succumbed following treatment with TNF alone. Strikingly, however, TNF and MRT co-treatment resulted in a highly significant reduction in survival, with 50% lethality only 8.5 h after injection and an overall survival of less than 20%. Importantly, concomitant RIPK1 inhibition completely prevented TNF and MRT-induced lethality (Fig. 5k). Hence, inhibition of RIPK1 by TBK1 and IKKε is essential for protection against TNF-induced lethal shock.

NEMO-recruited TANK and NAP1 engage TBK1 and IKKε to the TNFR1-SC. Having identified that the control of TNF-induced cell death by TBK1 and IKKε is essential, we determined the biochemical mechanism of their recruitment to complex-I. TBK1 and IKKε are known to associate with various adaptors that recruit them to different signalling platforms[29]. One such adaptor is TANK[51], which is recruited to complex-I in a HOIP-dependent manner (Fig. 1). Using TANK-deficient cells, we observed that IKKε recruitment was abrogated in these cells and that TBK1 recruitment was reduced but still occurred (Fig. 6a,b). Thus, IKKε recruitment entirely relies on TANK, whereas TBK1 is recruited by TANK and at least one additional adaptor.

After ruling out optineurin, a suggested TNFR1-SC component[52], as the protein responsible for TANK-independent TBK1 recruitment to complex-I (Supplementary Fig. 6a), we sought to identify the additional adaptor (or adaptors) for TBK1. We undertook this in an unbiased manner by studying the TBK1 interactome using TBK1-deficient cells re-expressing TAP-tagged TBK1 and performing an MS analysis on the affinity-purified TBK1. With NAP1, SINTBAD (also known as TBKBP1), TANK and TRAF2, this analysis only identified known TBK1 interactors[37] (Fig. 6c,d; Supplementary Table 5). While TRAF2 was recruited via TRADD independently of HOIP, and SINTBAD was not identified in the complex (Fig. 6e), NAP1 was recruited to complex-I in a LUBAC-dependent manner (Fig. 6e). In HeLa and A549 cells that had both TANK and NAP1 knocked out, we observed that TBK1 recruitment was completely or nearly completely absent from these cells, respectively (Fig. 6f; Supplementary Fig. 6b). In line with these results, the absence of TANK and NAP1 increased the autophosphorylation of RIPK1 in complex-I (Supplementary Fig. 6c). Thus, TANK and NAP1 are both responsible for the vast majority of TBK1 recruitment to complex-I.

As TANK has been shown to interact with NEMO[53], which is recruited to complex-I via M1 ubiquitin[36], we next evaluated the role of NEMO in TANK recruitment. This revealed that NEMO not only recruits TANK but also NAP1 and, consequently, brings IKKε and TBK1 to complex-I in both A549 cells and MEFs (Fig. 6g,h; Supplementary Fig. 6d). Moreover, re-expression of wild-type NEMO, but not of a deletion mutant unable to bind TANK[53] ($NEMO^{\Delta TBD}$), restored the recruitment of TANK, NAP1, TBK1 and IKKε to complex-I (Fig. 6i). Interestingly, IKKα and IKKβ deficiency or inhibition, as well as TAK1 inhibition, reduced TNF-induced TBK1 activation. The additional treatment with MRT further dampened this effect (Supplementary Fig. 6e–g). Thus, NEMO recruitment to complex-I, which is mostly, but not exclusively, M1 ubiquitin-dependent[34,36,54], recruits TANK and NAP1. TANK1 in turn brings TBK1 and IKKε, while NAP1 brings TBK1 to the TNFR1-SC. Their activation is partly dependent on IKKα and IKKβ and on autophosphorylation.

Together, these results show that NEMO mediates the recruitment of both canonical and non-canonical IKKs to complex-I, which all provide essential checkpoints to RIPK1, preventing untoward TNF-induced death.

Discussion

A major focus of current research on TNF-induced cell death is placed on the regulation of RIPK1, the central kinase in this process. Various post-translational modifications of RIPK1 are at the core of this regulation[50,55–58].

Currently, RIPK1 is thought to be kept in check in the cytosol under unstimulated conditions[59]. Following TNF stimulation, RIPK1 is recruited to complex-I[13], where it is rapidly post-translationally modified, including by cIAP1- and cIAP2-mediated K63-, K11- and K48-linked ubiquitylation and LUBAC-catalysed M1 ubiquitylation. M1 ubiquitin promotes the complex-I recruitment of NEMO together with its associated kinases, IKKα and IKKβ. Apart from activating NF-κB, IKKα and IKKβ inactivate RIPK1 by phosphorylation, preventing its translocation to complex-II. Recently, the existence of an additional cell death checkpoint involving the p38 MAPK target MK2 was described[18–20].

While TBK1 and IKKε were shown to be activated after TNF stimulation[45,52], their function in TNF signalling remained enigmatic. Here, we identified a NEMO-dependent checkpoint that controls TNF-induced cell death by the TBK1- and IKKε-mediated phosphorylation of RIPK1, which is largely dependent on M1 ubiquitylation and functionally independent from known cell death checkpoints (Supplementary Fig. 6h). It was recently proposed that the TBK1-mediated phosphorylation of RIPK1 on T189 impairs its substrate-binding capacity[60]. Our results, however, show that TBK1 and IKKε phosphorylate RIPK1 on multiple residues. It therefore appears that the TBK1- and IKKε-mediated regulation of RIPK1 is more complex. Further investigation will be required to define the contribution of the different TBK1- and IKKε-mediated phosphorylation events in keeping RIPK1 in check.

Interestingly, TBK1-deficient mice are embryonically lethal at embryonic day 14.5 due to aberrant TNFR1-induced cell death[30,31], a phenotype similar, but not identical, to that of NEMO-deficient animals[44,61]. Hence, it was initially assumed that TBK1 activates TNF-induced NF-κB-dependent gene expression. However, preventing TBK1 and IKKε activity exerts only limited effects on TNF-induced gene expression. Instead, we discovered that by phosphorylating RIPK1 on multiple sites within complex-I, TBK1 and IKKε control a physiologically essential cell death checkpoint. Accordingly, their pharmacological inhibition or genetic ablation resulted in TNF-induced cell death, both in cell lines and in vivo, as a consequence of unleashed RIPK1 activity and aberrant complex-II formation.

With the aim of elucidating the mechanism of how TBK1 and IKKε exert their function, we made the surprising discovery that NEMO mediates TBK1 and IKKε activation in complex-I. Mechanistically, NEMO enables the recruitment of TANK, which brings both TBK1 and IKKε to the complex, and of NAP1, which brings in additional TBK1. These results are striking, as they demonstrate that NEMO serves an essential survival function beyond regulating IKKα and IKKβ. Intriguingly, NEMO was previously shown to exert cell death-preventing functions independently of NF-κB[17,62]. Our results provide an explanation for this observation, as the combined activities of IKKα and IKKβ, TAK1 and MK2, and TBK1 and IKKε are required to keep RIPK1 in check. Of note, NEMO mutations are causative for a spectrum of diseases, including incontinentia pigmenti, ectodermal dysplasia and

immunodeficiency, which are thought to be caused by a deficiency in activating IKKα and IKKβ[63]. On the basis of our results, one may consider that aberrant TNF-induced cell death caused by the lack of TBK1 and IKKε activity may participate in disease progression in patients with certain NEMO mutations.

Our results prompt the question as to what could be the evolutionary advantage of having three distinct checkpoints all focused on RIPK1, a single component in the TNFR1 pathway. TNF is induced as one of the first cytokines in response to various cellular stressors[64]. It is tempting to speculate that this triple safeguard mechanism might serve to ensure that, should anything go wrong—perhaps as the result of a pathogen-mediated targeted intervention[65]—with any of three of the arguably most crucial signalling pathways for innate and adaptive immunity, this is sensed as early as possible during innate immune signalling. The inability to properly phosphorylate RIPK1 in response to TNF would serve this purpose, with the resulting outcome of TNF signalling, the untoward death of the cell, triggering an alternative route to inflammation.

We herein identified a crucial role for TBK1 and IKKε in preventing TNF-induced cell death. So far, these kinases have mainly been considered as modulators of gene expression, mostly in interferon responses[40,41] and autophagy[66,67]. However, certain pathologies have been associated with mutations or altered expression of TBK1 and IKKε, including neuroinflammatory diseases, for example amyotrophic lateral sclerosis or frontotemporal dementias[68], and various types of cancer[69]. Based on our results, diseases caused by NEMO deficiency should be added to this list. It will be interesting to evaluate to which extent aberrant TNF-induced, RIPK1-mediated cell death caused by deregulated TBK1 and IKKε activity participates in the initiation or progression of these diseases.

Online content

Any methods, additional references, Nature Research reporting summaries, source data, statements of data availability, and associated accession codes are available at https://doi.org/10.1038/s41556-018-0229-6.

Received: 20 December 2017; Accepted: 8 October 2018;
Published online: 12 November 2018

References

1. Micheau, O. & Tschopp, J. Induction of TNF receptor I-mediated apoptosis via two sequential signaling complexes. *Cell* **114**, 181–190 (2003).
2. Kalliolias, G. D. & Ivashkiv, L. B. TNF biology, pathogenic mechanisms and emerging therapeutic strategies. *Nat. Rev. Rheumatol.* **12**, 49–62 (2016).
3. Brenner, D., Blaser, H. & Mak, T. W. Regulation of tumour necrosis factor signalling: live or let die. *Nat. Rev. Immunol.* **15**, 362–374 (2015).
4. Hrdinka, M. & Gyrd-Hansen, M. The Met1-linked ubiquitin machinery: emerging themes of (de)regulation. *Mol. Cell* **68**, 265–280 (2017).
5. Shimizu, Y., Taraborrelli, L. & Walczak, H. Linear ubiquitination in immunity. *Immunol. Rev.* **266**, 190–207 (2015).
6. Kirisako, T. et al. A ubiquitin ligase complex assembles linear polyubiquitin chains. *EMBO J.* **25**, 4877–4887 (2006).
7. Ikeda, F. et al. SHARPIN forms a linear ubiquitin ligase complex regulating NF-kappaB activity and apoptosis. *Nature* **471**, 637–641 (2011).
8. Gerlach, B. et al. Linear ubiquitination prevents inflammation and regulates immune signalling. *Nature* **471**, 591–596 (2011).
9. Tokunaga, F. et al. SHARPIN is a component of the NF-kappaB-activating linear ubiquitin chain assembly complex. *Nature* **471**, 633–636 (2011).
10. Peltzer, N. et al. HOIP deficiency causes embryonic lethality by aberrant TNFR1-mediated endothelial cell death. *Cell Rep.* **9**, 153–165 (2014).
11. Emmerich, C. H. et al. Activation of the canonical IKK complex by K63/M1-linked hybrid ubiquitin chains. *Proc. Natl Acad. Sci. USA* **110**, 15247–15252 (2013).
12. Peltzer, N. et al. LUBAC is essential for embryogenesis by preventing cell death and enabling haematopoiesis. *Nature* **557**, 112–117 (2018).
13. Haas, T. L. et al. Recruitment of the linear ubiquitin chain assembly complex stabilizes the TNF-R1 signaling complex and is required for TNF-mediated gene induction. *Mol. Cell* **36**, 831–844 (2009).
14. Draber, P. et al. LUBAC-recruited CYLD and A20 regulate gene activation and cell death by exerting opposing effects on linear ubiquitin in signaling complexes. *Cell Rep.* **13**, 2258–2272 (2015).
15. Kupka, S., Reichert, M., Draber, P. & Walczak, H. Formation and removal of poly-ubiquitin chains in the regulation of tumor necrosis factor-induced gene activation and cell death. *FEBS J.* **283**, 2626–2639 (2016).
16. Rahighi, S. et al. Specific recognition of linear ubiquitin chains by NEMO is important for NF-kappaB activation. *Cell* **136**, 1098–1109 (2009).
17. Dondelinger, Y. et al. NF-kappaB-independent role of IKKalpha/IKKbeta in preventing RIPK1 kinase-dependent apoptotic and necroptotic cell death during TNF signaling. *Mol. Cell* **60**, 63–76 (2015).
18. Menon, M. B. et al. p38MAPK/MK2-dependent phosphorylation controls cytotoxic RIPK1 signalling in inflammation and infection. *Nat. Cell Biol.* **19**, 1248–1259 (2017).
19. Jaco, I. et al. MK2 phosphorylates RIPK1 to prevent TNF-induced cell death. *Mol. Cell* **66**, 698–710 (2017).
20. Dondelinger, Y. et al. MK2 phosphorylation of RIPK1 regulates TNF-mediated cell death. *Nat. Cell Biol.* **19**, 1237–1247 (2017).
21. Kotlyarov, A. et al. MAPKAP kinase 2 is essential for LPS-induced TNF-alpha biosynthesis. *Nat. Cell Biol.* **1**, 94–97 (1999).
22. Kanayama, A. et al. TAB2 and TAB3 activate the NF-kappaB pathway through binding to polyubiquitin chains. *Mol. Cell* **15**, 535–548 (2004).
23. Wang, C. et al. TAK1 is a ubiquitin-dependent kinase of MKK and IKK. *Nature* **412**, 346–351 (2001).
24. Adhikari, A., Xu, M. & Chen, Z. J. Ubiquitin-mediated activation of TAK1 and IKK. *Oncogene* **26**, 3214–3226 (2007).
25. Wu, C. J., Conze, D. B., Li, T., Srinivasula, S. M. & Ashwell, J. D. Sensing of Lys 63-linked polyubiquitination by NEMO is a key event in NF-kappaB activation [corrected]. *Nat. Cell Biol.* **8**, 398–406 (2006).
26. Salmeron, A. et al. Direct phosphorylation of NF-kappaB1p105 by the IkappaB kinase complex on serine 927 is essential for signal-induced p105 proteolysis. *J. Biol. Chem.* **276**, 22215–22222 (2001).
27. Tojima, Y. et al. NAK is an IkappaB kinase-activating kinase. *Nature* **404**, 778–782 (2000).
28. Peters, R. T., Liao, S. M. & Maniatis, T. IKKepsilon is part of a novel PMA-inducible IkappaB kinase complex. *Mol. Cell* **5**, 513–522 (2000).
29. Helgason, E., Phung, Q. T. & Dueber, E. C. Recent insights into the complexity of Tank-binding kinase 1 signaling networks: the emerging role of cellular localization in the activation and substrate specificity of TBK1. *FEBS Lett.* **587**, 1230–1237 (2013).
30. Hemmi, H. et al. The roles of two IkappaB kinase-related kinases in lipopolysaccharide and double stranded RNA signaling and viral infection. *J. Exp. Med.* **199**, 1641–1650 (2004).
31. Perry, A. K., Chow, E. K., Goodnough, J. B., Yeh, W. C. & Cheng, G. Differential requirement for TANK-binding kinase-1 in type I interferon responses to toll-like receptor activation and viral infection. *J. Exp. Med.* **199**, 1651–1658 (2004).
32. Kupka, S. et al. SPATA2-mediated binding of CYLD to HOIP enables CYLD recruitment to signaling complexes. *Cell Rep.* **16**, 2271–2280 (2016).
33. Komander, D. et al. Molecular discrimination of structurally equivalent Lys 63-linked and linear polyubiquitin chains. *EMBO Rep.* **10**, 466–473 (2009).
34. Laplantine, E. et al. NEMO specifically recognizes K63-linked poly-ubiquitin chains through a new bipartite ubiquitin-binding domain. *EMBO J.* **28**, 2885–2895 (2009).
35. Ea, C. K., Deng, L., Xia, Z. P., Pineda, G. & Chen, Z. J. Activation of IKK by TNFalpha requires site-specific ubiquitination of RIP1 and polyubiquitin binding by NEMO. *Mol. Cell* **22**, 245–257 (2006).
36. Hadian, K. et al. NF-kappaB essential modulator (NEMO) interaction with linear and Lys-63 ubiquitin chains contributes to NF-kappaB activation. *J. Biol. Chem.* **286**, 26107–26117 (2011).
37. Chau, T. L. et al. Are the IKKs and IKK-related kinases TBK1 and IKK-epsilon similarly activated? *Trends Biochem. Sci.* **33**, 171–180 (2008).
38. Kishore, N. et al. IKK-i and TBK-1 are enzymatically distinct from the homologous enzyme IKK-2: comparative analysis of recombinant human IKK-i, TBK-1, and IKK-2. *J. Biol. Chem.* **277**, 13840–13847 (2002).
39. Lafont, E. et al. The linear ubiquitin chain assembly complex regulates TRAIL-induced gene activation and cell death. *EMBO J.* **36**, 1147–1166 (2017).
40. Fitzgerald, K. A. et al. IKKepsilon and TBK1 are essential components of the IRF3 signaling pathway. *Nat. Immunol.* **4**, 491–496 (2003).
41. Sharma, S. et al. Triggering the interferon antiviral response through an IKK-related pathway. *Science* **300**, 1148–1151 (2003).
42. Clement, J. F., Meloche, S. & Servant, M. J. The IKK-related kinases: from innate immunity to oncogenesis. *Cell Res.* **18**, 889–899 (2008).
43. Clark, K. et al. Novel cross-talk within the IKK family controls innate immunity. *Biochem. J.* **434**, 93–104 (2011).
44. Schmidt-Supprian, M. et al. NEMO/IKK gamma-deficient mice model incontinentia pigmenti. *Mol. Cell* **5**, 981–992 (2000).

45. Clark, K., Plater, L., Peggie, M. & Cohen, P. Use of the pharmacological inhibitor BX795 to study the regulation and physiological roles of TBK1 and IkappaB kinase epsilon: a distinct upstream kinase mediates Ser-172 phosphorylation and activation. *J. Biol. Chem.* **284**, 14136–14146 (2009).
46. Feng, S. et al. Cleavage of RIP3 inactivates its caspase-independent apoptosis pathway by removal of kinase domain. *Cell. Signal.* **19**, 2056–2067 (2007).
47. Lin, Y., Devin, A., Rodriguez, Y. & Liu, Z. G. Cleavage of the death domain kinase RIP by caspase-8 prompts TNF-induced apoptosis. *Genes Dev.* **13**, 2514–2526 (1999).
48. O'Donnell, M. A. et al. Caspase 8 inhibits programmed necrosis by processing CYLD. *Nat. Cell Biol.* **13**, 1437–1442 (2011).
49. Duprez, L. et al. RIP kinase-dependent necrosis drives lethal systemic inflammatory response syndrome. *Immunity* **35**, 908–918 (2011).
50. Polykratis, A. et al. Cutting edge: RIPK1 kinase inactive mice are viable and protected from TNF-induced necroptosis in vivo. *J. Immunol.* **193**, 1539–1543 (2014).
51. Pomerantz, J. L. & Baltimore, D. NF-kappaB activation by a signaling complex containing TRAF2, TANK and TBK1, a novel IKK-related kinase. *EMBO J.* **18**, 6694–6704 (1999).
52. Wagner, S. A., Satpathy, S., Beli, P. & Choudhary, C. SPATA2 links CYLD to the TNF-α receptor signaling complex and modulates the receptor signaling outcomes. *EMBO J.* **35**, 1868–1884 (2016).
53. Chariot, A. et al. Association of the adaptor TANK with the I kappa B kinase (IKK) regulator NEMO connects IKK complexes with IKK epsilon and TBK1 kinases. *J. Biol. Chem.* **277**, 37029–37036 (2002).
54. Dynek, J. N. et al. c-IAP1 and UbcH5 promote K11-linked polyubiquitination of RIP1 in TNF signalling. *EMBO J.* **29**, 4198–4209 (2010).
55. Wang, L., Du, F. & Wang, X. TNF-alpha induces two distinct caspase-8 activation pathways. *Cell* **133**, 693–703 (2008).
56. Peltzer, N., Darding, M. & Walczak, H. Holding RIPK1 on the ubiquitin leash in TNFR1 signaling. *Trends Cell Biol.* **26**, 445–461 (2016).
57. Annibaldi, A. & Meier, P. Checkpoints in TNF-induced cell death: implications in inflammation and cancer. *Trends Mol. Med.* **24**, 49–65 (2018).
58. Ting, A. T. & Bertrand, M. J. More to life than NF-kappaB in TNFR1 signaling. *Trends Immunol.* **37**, 535–545 (2016).
59. Vanden Berghe, T., Kalai, M., van Loo, G., Declercq, W. & Vandenabeele, P. Disruption of HSP90 function reverts tumor necrosis factor-induced necrosis to apoptosis. *J. Biol. Chem.* **278**, 5622–5629 (2003).
60. Xu, D. et al. TBK1 suppresses RIPK1-driven apoptosis and inflammation during development and in aging. *Cell* **174**, 1477–1491 (2018).
61. Rudolph, D. et al. Severe liver degeneration and lack of NF-kappaB activation in NEMO/IKKgamma-deficient mice. *Genes Dev.* **14**, 854–862 (2000).
62. Legarda-Addison, D., Hase, H., O'Donnell, M. A. & Ting, A. T. NEMO/IKKgamma regulates an early NF-kappaB-independent cell-death checkpoint during TNF signaling. *Cell Death Differ.* **16**, 1279–1288 (2009).
63. Maubach, G., Schmadicke, A. C. & Naumann, M. NEMO links nuclear factor-kappaB to human diseases. *Trends Mol. Med.* **23**, 1138–1155 (2017).
64. Udalova, I., Monaco, C., Nanchahal, J. & Feldmann, M. Anti-TNF Therapy. *Microbiol. Spectr.* https://doi.org/10.1128/microbiolspec.MCHD-0022-2015 (2016).
65. Zhao, W. Negative regulation of TBK1-mediated antiviral immunity. *FEBS Lett.* **587**, 542–548 (2013).
66. Thurston, T. L., Ryzhakov, G., Bloor, S., von Muhlinen, N. & Randow, F. The TBK1 adaptor and autophagy receptor NDP52 restricts the proliferation of ubiquitin-coated bacteria. *Nat. Immunol.* **10**, 1215–1221 (2009).
67. Pilli, M. et al. TBK-1 promotes autophagy-mediated antimicrobial defense by controlling autophagosome maturation. *Immunity* **37**, 223–234 (2012).
68. Ahmad, L., Zhang, S. Y., Casanova, J. L. & Sancho-Shimizu, V. Human TBK1: a gatekeeper of neuroinflammation. *Trends Mol. Med.* **22**, 511–527 (2016).
69. Verhelst, K., Verstrepen, L., Carpentier, I. & Beyaert, R. IkappaB kinase epsilon (IKKepsilon): a therapeutic target in inflammation and cancer. *Biochem. Pharmacol.* **85**, 873–880 (2013).
70. Vizcaino, J. A. et al. 2016 update of the PRIDE database and its related tools. *Nucleic Acids Res.* **44**, 11033 (2016).

Acknowledgements

The authors thank all members of the Walczak Group for useful technical advice and fruitful scientific discussions, and A. Betrancourt and J. Kadluczka for excellent technical support. They also thank the following: M. Bertrand for IKKα and IKKβ knockout MEFs; M. Pasparakis for NEMO knockout MEFs; J. Bertin for RIPK1 kinase-dead MEFs; and T. Brooks from the ICH Genetics & Genomic Medicine Programme (London, UK) for RNA-seq services. This work was supported by a Wellcome Trust Investigator Award (096831/Z/11/Z), an ERC Advanced Grant (294880) and a Cancer Research UK programme grant (A17341) awarded to H.W., a Czech Science Foundation grant (17-27355Y) awarded to P.D., and a BBSRC CASE studentship (BB/J013129/1) awarded to M.R. This work also received support from a CRUK–UCL Centre grant (C416/A25145), the CRUK Cancer Immunotherapy Network Accelerator (CITA) Award (C33499/A20265), and the National Institute for Health Research University College London Hospitals Biomedical Research Centre.

Author contributions

H.W. conceived the project. E.L., P.D., E.R., M.R., S.K., A.v.M. and A.L. designed and performed the experiments and analysed the data. S.S., A.B. and K.W. performed the MS experiments and analysed the obtained data. S.S. supervised the MS experiments. H.D. and A.C. performed experiments. D.d.M. generated essential tools for the study. S.H. analysed the RNA-seq data. E.L., E.R., P.D. and H.W. wrote the manuscript.

Competing interests

H.W. is a co-founder and shareholder of Apogenix AG. All other authors have no competing interests.

Additional information

Supplementary information is available for this paper at https://doi.org/10.1038/s41556-018-0229-6.

Reprints and permissions information is available at www.nature.com/reprints.

Correspondence and requests for materials should be addressed to H.W.

Publisher's note: Springer Nature remains neutral with regard to jurisdictional claims in published maps and institutional affiliations.

Methods

Recombinant proteins, cells and cell lines. Human full-length GST (glutathione *S*-transferase)-RIPK1 was from Abnova, GST-IKKε was from ThermoFisher and GST-TBK1 was from Sigma-Aldrich. Untagged TNF, HA (human influenza hemagglutinin)-TNF and TAP-TNF were produced and purified as previously described[14]. Etanercept was purchased from Pfizer.

Wild-type cancer cell lines were purchased from the American Type Culture Collection. The generation and reconstitution of cancer cell lines with HOIP, TANK, NAP1, optineurin, NEMO, TBK1 and IKKε, or TNF knocked out, and the generation of the different knockout MEFs were performed as previously described[10,14]. The single guide RNA sequences used are presented in Supplementary Table 6. Newly generated knockout cells were validated by sequencing. A549 and HeLa cells were transduced to express a TAP-tagged form of RIPK3. Briefly, we used a carboxy-terminal TAP-tag consisting of a 2× Strep-tag II sequence followed by a PreScission cleavage site and 1× Flag-tag. The coding sequence of human RIPK3 was inserted into the retroviral MSCV vector, followed by an internal ribosome entry site and the open reading frame of enhanced green fluorescent protein (EGFP). This vector was transfected using Lipofectamine 2000 in Phoenix-AMPHO cells. One day after transfection, the medium was replaced, and viral supernatants were collected at days 2 and 3. Viral supernatants were passed through a 0.45-µm filter, added to HeLa or A549 cells at 60% confluence in the presence of polybrene (6 µg ml^{-1}) before cells were subjected to spinfection (1300 × g, 45 min, 30 °C). EGFP-positive cells were isolated using MoFlo FACS (Beckman Coulter) to more than 95% purity 2 days after infection. HOIP knockout HeLa and A549 cells re-expressing HOIP^{WT}, HOIP^{C885S}, Empty pBabe or the MSCV vector, as well as TBK1 knockout A549 cells re-expressing TBK1^{WT} or TBK1^{D135N}, were generated as previously described[39]. A549 NEMO knockout cells were transduced with pBabe-puro to re-express NEMO^{WT} or NEMO$^{\Delta TBD}$ (200–250 amino acid deletion). Corresponding primers can be found in Supplementary Table 6. All cell lines were regularly tested for mycoplasma using a MycoAlert Mycoplasma Detection kit (Lonza).

Inhibitors and antibodies. The following inhibitors were used at the indicated final concentration in vitro, unless otherwise specified in the figure or figure legends: MRT (2 µM; Sigma-Aldrich); BX-795 (1 µM; Invivogen); TPCA-1 (5 µM; Tocris Bioscience); PF-3644022 (1 µM; Tocris Bioscience); 7-oxozeanol (1 µM; Tocris Bioscience); Nec-1s (10 µM; Biovision); zVAD-FMK (20 µM; Abcam); cycloheximide (0.5 µg ml^{-1}; Sigma-Aldrich).

All antibodies used in this study are listed in Supplementary Table 7, including information regarding dilutions and validation.

Retroviral transduction of cells. Coding sequences of HOIP^{WT}, HOIP^{C885S}, TBK1^{WT} or TBK1^{D135N} were inserted into the retroviral MSCV vector containing GFP as the selection marker. Following infection, cells were sorted using MoFlo FACS (Beckman Coulter).

Tandem affinity purification. Samples were directly lysed in the case of TBK1-TAP-expressing cells or corresponding control cells. For A549 cells expressing HOIP^{WT} or with HOIP knocked out (7.5×10^8 cells each), cells were first stimulated with TAP-TNF for 15 min. Cells were subsequently solubilized in IP lysis buffer (30 mM Tris-HCl pH 7.4, 120 mM NaCl, 2 mM EDTA, 2 mM KCl, 10% glycerol, 1% n-dodecyl-β-maltoside, 50 mM NaF, 5 mM Na_3VO_4, 1× Complete protease-inhibitor cocktail (Roche)) and cleared by centrifugation (13,000 r.p.m., 30 min, 4 °C). Samples were then incubated overnight with 100 µl of anti-Flag M2-Agarose beads (Sigma) and washed three times with IP lysis buffer. Proteins were eluted overnight in IP lysis buffer containing 150 µg ml^{-1} 3× Flag peptide (Sigma) and 20 U ml^{-1} PreScission Protease (GE Healthcare). Samples were subsequently subjected to a second affinity precipitation step using Strep-Tactin resin (QIAGEN) overnight at 4 °C and eluted with 5 mM biotin. Proteins were precipitated using a 2-D Clean-Up kit (GE Healthcare) and resuspended in ice-cold denaturation buffer (100 mM ammonium bicarbonate, 8 M urea). The samples were then reduced with 4 mM dithiothreitol (DTT) at 56 °C for 30 min, alkylated with 8 mM iodoacetamide at 22 °C in the dark, and 4 mM DTT was used to neutralize the excess of iodoacetamide. Proteins were digested first with endoproteinase Lys-C (Wako Chemicals) for 4 h at 37 °C. Subsequently, samples were diluted with 2 M urea, and further digested with sequencing-grade trypsin (Promega) for 15 h at 37 °C. Samples were desalted with microspin columns filled with SEM SS18V silica (The Nest Group), eluted with 50% acetonitrile 0.1% trifluoroacetic acid, evaporated to dryness at 30 °C, and resolubilized in 20 µl water containing 10% formic acid. A total of 1 µl of the resulting peptidic solution was used for liquid chromatography (LC)–MS analysis.

In vitro kinase assays. For the IKKε in vitro kinase assays, 250 ng of recombinant RIPK1 and 125 ng of recombinant IKKε were mixed in 30 µl kinase buffer (20 mM HEPES pH 7.5, 10 mM $MgCl_2$, 2 mM DTT, phosphatase inhibitor (PhosSTOP), EDTA-free protease inhibitor cocktail, 20 µM ATP) and incubated for 30 min at 30 °C. For the TBK1 in vitro kinase assays, equal amounts of recombinant proteins were used (for example, 250 ng) of recombinant RIPK1 and TBK1. The incubation time was 2 h at 30 °C. The kinase buffer used was the same as for the IKKε kinase assay but included 100 mM NaCl and the ATP concentration was 100 µM. Kinase reactions were denatured by the addition of 4× reducing sample buffer (200 µM DTT).

For the MS experiment, 2 µg of recombinant RIPK1 and 1 µg of recombinant IKKε were used, and the assay was performed as described above. Proteins were separated and purified on an SDS–polyacrylamide gel electrophoresis (PAGE) gel. Respective protein bands were excised, and proteins were reduced with 5 mM tris(2-carboxyethyl)phosphine (TCEP) in 50 mM triethylammonium bicarbonate (TEAB) at 37 °C for 20 min, alkylated with 10 mM chloroacetamide in 50 mM TEAB at ambient temperature for 20 min in the dark, and digested with 1:10 trypsin to protein ratio in-gel at 37 °C for 4 h. Protein gel bands were redigested to extract any remaining peptides. Samples were evaporated to dryness at 30 °C and resolubilized in 0.1% formic acid.

Mass spectrometry. nLC–MS/MS was performed using a Q Exactive Orbitrap Plus interfaced to a Nanospray Flex ion source and coupled to an Easy-nLC 1000 (Thermo Scientific). Peptides were separated on a 24-cm fused silica emitter, 75-µm diameter, packed in-house with Reprosil-Pur 200 C18-AQ, 2.4-µm resin (Dr. Maisch) using a linear gradient from 5% to 30% acetonitrile/0.1% formic acid over 10 min (for TBK1 affinity purification (AP)-MS) or 30 min (for TNFR-SC AP-MS and kinase assays) at a flow rate of 250 nl min^{-1}. Precursor ions were measured in a data-dependent mode in the orbitrap analyser at a resolution of 70,000 and a target value of 3×10^6 ions. The ten most intense ions from each MS1 scan were isolated, fragmented in the higher-energy collisional dissociation cell, and measured in the orbitrap at a resolution of 17,500. The proteomic raw data have been deposited in the ProteomeXchange Consortium via the PRIDE[70] partner repository with the dataset identifiers PXD008497 (TNFR1-SC analysis), PXD010777 (TBK1 analysis) and PXD008518 (RIPK1 kinase assay). Analyses of these data are provided in Supplementary Tables 2, 4 and 5.

Protein and phosphosite identification. Raw data were analysed using MaxQuant v.1.5.2.8, where they were searched against the human UniProt database (http://www.uniprot.org/, downloaded 22 Oct 2015 (for TNFR-SC AP-MS) and 5 Oct 2017 (for TBK1 AP-MS and kinase assays)) using default settings. Carbamidomethylation of cysteine residues was set as the fixed modification, and oxidation of methionine residues and acetylation at amino termini were set as the variable modifications. Phosphorylation (STY) was set as a variable modification for the kinase assays. Enzyme specificity was set to trypsin with maximally two missed cleavages allowed. To ensure high confidence identifications, peptide-spectrum matches, peptides and proteins were filtered at a less than 1% false discovery rate. Proteins identified with a single peptide were filtered out. Label-free quantification in MaxQuant was used to quantify the AP-MS data.

Processing of TNFR1-SC AP-MS data. Proteins quantified in unstimulated controls were regarded as contaminants and filtered out. Proteins detected in more than 15 experiments in the Contaminant Repository for Affinity Purification Mass Spectrometry Data (CRAPome) were filtered out. Proteins not present in the TNF-stimulated parental cells were filtered out. A protein–protein interaction network was generated in the STRING protein–protein interaction database using known interactions from curated databases and experimentally determined using default settings. Proteins not connected in the interaction network were filtered out.

Processing of TBK1 AP-MS data. Proteins quantified in TBK1 knockout cells were filtered out. Proteins detected in more than 15 experiments in the CRAPome were filtered out. A protein–protein interaction network was generated in the STRING protein–protein interaction database using known interactions from curated databases and experimentally determined using default settings. Proteins not connected in the interaction network were filtered out.

Processing of RIPK1 kinase assay data. Three raw files for each sample type (50% of the first digestion, 10% of the second digestion and 90% of the second digestion) were searched and grouped in MaxQuant to produce one output file. Non-RIPK1 phosphosites were filtered out from the 'phosphoSTY.txt' results file. Phosphorylation profiles of RIPK1 with and without IKKε were compared. Phosphosites detected in RIPK1 + IKKε that were absent from RIPK1 alone were taken forward. Phosphosite localization was carried out using the 'Phospho (STY) Probabilities' column. Serine, threonine or tyrosine residues with the following probability values were identified as follows: probabilities of <0.1 were considered not likely to be phosphorylated; probabilities of ≥0.1 and <0.75 were considered to be possible phosphosites; and probabilities of ≥0.75 were considered to be likely phosphosites.

Cell activation and immunoprecipitation. For TNFR1-SC preparation, cells were washed with PBS, resuspended in serum-free medium and stimulated with FLAG-TNF or TAP-TNF for the indicated times. Cells were lysed in IP lysis buffer at 4 °C for 1 h. FLAG-TNF or TAP-TNF (500 ng) was added to the lysates of non-stimulated control samples. Subsequently, the lysates were centrifuged at 13,300 r.p.m. for 20 min and the TNFR1-SC was immunoprecipitated using M2-Agarose beads (Sigma) overnight at 4 °C. The following day, the beads were washed three times with IP lysis buffer (1 ml), and proteins were eluted by

boiling in reducing sample buffer. Samples were analysed by western blotting. For the isolation of retrovirally expressed TAP-tagged proteins, cells were stimulated with untagged TNF as indicated and subjected to immunoprecipitation with M2-Agarose beads. Immunoprecipitation with specific antibodies for RIPK1 (BD, 610459) or FADD (Santa Cruz, H-181) was performed by antibody-coupling to protein A/G-Agarose beads (Santa Cruz) for 3 h at room temperature. Deubiquitylation and/or dephosphorylation was performed on some immunoprecipitates as indicated in the figure legends. For deubiquitylation, beads were resuspended in DUB buffer (50 mM HEPES pH 7.6, 150 mM NaCl, 5 mM DTT) and 1 µM of the recombinant deubiquitinase USP2 (Boston Biochem) was added. The assay was performed at 30 °C for 1 h. For samples in which the additional removal of phosphorylation was carried out, 400 U of λ-phosphatase was added where indicated and reactions were further incubated at 37 °C for 30 min.

SDS–PAGE and western blotting. Proteins were separated using 4–15% Mini- or Midi-Protean-TGX gels (Bio-Rad) with Tris–glycine–SDS running buffer. Proteins were transferred on Mini or Midi 0.2-µm nitrocellulose membranes (Bio-Rad transfer packs) using a Trans-Blot Turbo Transfer System from Bio-Rad. Proteins were detected using antibodies as indicated.

Isolation of BMDMs. For the preparation of BMDMs, 6–12-week-old mice were killed. Hind legs were removed and bones were separated from muscle tissue. Femur and tibia were opened on each side, and bone marrow was flushed using a 25-gauge needle and syringe. Cells were then resuspended in RPMI medium containing 10% fetal calf serum, 1% penicillin–streptomycin (Invitrogen) and 10% conditioned medium from L929 cells and passed through a cell strainer. Subsequently, cells were plated in a 12- or 24-well plate. The conditioned medium was replaced every 2 days, and cells were incubated for 7 days before the experiment.

RNA-seq analysis. A549 wild-type cells were pretreated with vehicle (dimethylsulfoxide (DMSO)), MRT or TPCA-1 followed by TNF stimulation (200 ng ml^{-1}) for 0, 1 or 4 h. Triplicates for each stimulation time and type of treatment were performed. Cells were then lysed and their total RNA extracted using a RNeasy Mini kit (Qiagen, 74104) according to the manufacturer's instructions. To generate the library, samples were processed using a KAPA mRNA HyperPrep kit (KK8580) according to the manufacturer's instructions. Briefly, mRNA was isolated from total RNA using Oligo dT beads to pull down polyadenylated transcripts. The purified mRNA was fragmented using chemical hydrolysis (heat and divalent metal cations) and primed with random hexamers. Strand-specific first strand complementary DNA was generated using reverse transcriptase in the presence of actinomycin D. The second cDNA strand was synthesized using dUTP in place of dTTP to mark the second strand. The resultant cDNA was then 'A-tailed' at the 3′ end to prevent self-ligation and adapter dimerization. Truncated adaptors, containing a T overhang, were ligated to the A-tailed cDNA. Successfully ligated cDNA molecules were then enriched by limited cycle PCR. All pipetting steps and incubations were performed by automation on a Hamilton StarLet liquid handler, with the exception of the high temperature fragmentation and the limited cycle PCR. Libraries to be multiplexed in the same run were pooled in equimolar quantities, calculated from Qubit and Bioanalyser fragment analyses. Samples were sequenced on a NextSeq 500 instrument (Illumina) using either a 43-bp or 81-bp paired end run. Run data were demultiplexed and converted to fastq files using Illumina's bcl2fastq Conversion software v.2.19. Next, the expression of Illumina paired RNA-seq transcript counts was quantified using kallisto software and a GRCh38 transcript model. The data were imported to the R statistical environment and summarized at the gene level (that is, transcript counts summed) using tximport. Statisical transformations (for example, the rlog used in Fig. 2c and Supplementary Fig. 2c) and analyses of differential expression were performed using DESeq2. Multiple testing adjustments of differential expression utilized the Benjamini–Hochberg and independent hypothesis weighting (IHW) adjustments. Transcripts that were significantly changed between 0 and 1 h of TNF stimulation in each group (control, MRT-treated and TPCA-1-treated) were illustrated using BioVenn software.

The RNA-seq raw dataset generated during the current study is available in the SRA repository and can be accessed using the BioProject accession number PRJNA422567 or the SRA accession number SRP126844 (https://www.ncbi.nlm.nih.gov/Traces/study/?acc=SRP126844). The specific analysis of transcripts that significantly changed at 1 h (corresponding to Fig. 2d) is provided in Supplementary Table 3.

Cell death analysis. Cells were seeded the day before the experiment at 90,000 cells per well in a 24-well plate or at 150,000 cells per well in a 12 well plate. The following day, cells were pretreated with the indicated inhibitors and treated with recombinant human TNF (50 ng ml^{-1} to 500 ng ml^{-1}) in the presence of 5 µM Sytox Green (ThermoFisher). Dead cells were imaged in real-time for the indicated duration of time in either 1 h or 2 h intervals via fluorescence signals using an IncuCyte FLR. The percentage of cell death was calculated by manually counting the number of dead cells from a representative image recorded at the last time point for each sample using ImageJ.

CellTiter-Glo luminescent cell viability assay. Cells were seeded the day before the experiment at either 10,000 cells per well in a 96-well plate in triplicate or at 90,000 cells per well in a 24-well plate. The next day, cells were pretreated with the indicated inhibitors followed by treatment with recombinant human TNF (50 ng ml^{-1} for L929, 500 ng ml^{-1} for MEFs, or at the indicated dose). Cells were subsequently lysed and treated according to the manufacturer's instructions. Luminescence was measured using a Mithras LB 940 Multimode Microplate Reader, and viability was calculated via normalization to untreated samples.

2D gel electrophoresis. TNFR1-SC was eluted from M2-Agarose beads in 300 µl lysis buffer containing 5 U ml^{-1} PreScission (GE Healthcare Life Sciences) and 250 mg ml^{-1} 3× FLAG-peptide (Sigma) for 12 h at 4 °C. A second elution step was carried out for 6 h, and both elution volumes were pooled. Eluted TNFR1-SC was then prepared for 2D electrophoresis by using a 2-D Clean-Up kit (GE Healthcare Life Sciences). The pellet from the clean-up step was resuspended in 125 µl 2D rehydration solution (7 M urea, 2 M thiourea, 4% CHAPS (3-((3-cholamidopropyl) dimethylammonio)-1-propanesulfonate), 0.5% carrier ampholyte (IPG buffer of respective pH), 20 mM DTT, 0.002% bromophenol blue), before being loaded by cup loading onto either pH 3–10NL or pH 4–7 rehydrated 7-cm Immobiline Drystrips (GE Healthcare) and run on an Ettan IPGphor 3 system using the manufacturer's recommended settings. The Immobiline strip was then washed with equilibration buffer (GE Healthcare) containing 65 mM DTT and 135 mM iodoacetamide for 15 min each. Equilibrated gel strips were then loaded and run on NuPAGE 4–12% Bis-Tris ZOOM Protein Gels, followed by western blotting.

Mice injections and monitoring for TNF-α-induced shock. Six- to eight-week old female C57BL/6N mice each received two intraperitoneal injections (total volume of 300 µl per mouse) at 15 min intervals of vehicle, Nec-1s (120 µg), MRT (300 µg) or a combination thereof, followed by one intravenous injection (total volume of 150 µl per mouse) of vehicle or murine TNF (5 µg). Inhibitors and TNF were reconstituted and diluted in endotoxin-free PBS. Animals were under permanent observation. Six to ten mice were used per group, as specifically indicated for each experiment. The study protocol used for the animal experiments and for the use of the TNF-induced shock model was obtained from the German Approval of Animal Act committee (application no. V244-7224.121-4). All in vivo experiments were performed according to institutional, national and European ethical animal regulations (Protection of Animals Act).

Statistics and reproducibility. For the vast majority of the western blot analyses, results shown are representative of at least two independent experiments, as indicated in each legend. All statistical analyses were performed using GraphPad Prism v.6 software (Graphpad). Cell death data are presented as relative fluorescent units (RFU) mean of technical replicates of Sytox Green-positive cells for one representative experiment out of three independent experiments, as specified in the legends. For the loss of viability data, values are expressed as the mean percentage of loss of viability ± s.d. for three to four independent experiments as specified for each panel in the legends. Survival curves for the in vivo experiment were compared using log-rank Mantel–Cox tests. The significance between the samples is indicated in the figure. For the RNA-seq experiments, statistical analyses are specified in the "RNA-seq analysis" section.

Code availability. For the RNA-seq analysis, the data were imported to the R statistical environment and summarized at the gene level (that is, transcript counts summed) using tximport. Statisical transformations (for example, the rlog used in Fig. 2c and Supplementary Fig. 2c) and the analysis of differential expression was performed using DESeq2. Multiple testing adjustments of differential expression utilized the Benjamini–Hochberg and IHW adjustments. The corresponding computational code for analysis is available upon request directly with the corresponding author.

Reporting Summary. Further information on research design is available in the Nature Research Reporting Summary linked to this article.

Data availability

The raw data for RNA-seq analysis (Fig. 2; Supplementary Fig. 2c; Supplementary Table 3) and the proteomic raw data (Figs. 1a and 5f; Supplementary Tables 2, 4 and 5) are available as described below. The RNA-seq raw dataset generated during the current study are available in the SRA repository and can be accessed using the BioProject accession number PRJNA422567 or the SRA accession number SRP126844 (https://www.ncbi.nlm.nih.gov/Traces/study/?acc=SRP126844). The proteomic raw data have been deposited in the ProteomeXchange Consortium via the PRIDE[70] partner repository with the dataset identifiers PXD008497 (TNFR1-SC analysis), PXD010777 (TBK1 analysis) and PXD008518 (RIPK1 kinase assay). Source data for the graphs of all the other experiments in this study are available in Supplementary Table 1, and unprocessed scans for western blots are displayed in Supplementary Fig. 7. Publicly available tools were used for RNA-seq analysis as specified in the online methods, and the corresponding computational code is available upon request directly with the authors.

nature research

Corresponding author(s): Henning Walczak

Reporting Summary

Nature Research wishes to improve the reproducibility of the work that we publish. This form provides structure for consistency and transparency in reporting. For further information on Nature Research policies, see Authors & Referees and the Editorial Policy Checklist.

Statistical parameters

When statistical analyses are reported, confirm that the following items are present in the relevant location (e.g. figure legend, table legend, main text, or Methods section).

n/a	Confirmed	
☐	☒	The exact sample size (*n*) for each experimental group/condition, given as a discrete number and unit of measurement
☐	☒	An indication of whether measurements were taken from distinct samples or whether the same sample was measured repeatedly
☐	☒	The statistical test(s) used AND whether they are one- or two-sided *Only common tests should be described solely by name; describe more complex techniques in the Methods section.*
☒	☐	A description of all covariates tested
☐	☒	A description of any assumptions or corrections, such as tests of normality and adjustment for multiple comparisons
☐	☒	A full description of the statistics including central tendency (e.g. means) or other basic estimates (e.g. regression coefficient) AND variation (e.g. standard deviation) or associated estimates of uncertainty (e.g. confidence intervals)
☐	☒	For null hypothesis testing, the test statistic (e.g. *F*, *t*, *r*) with confidence intervals, effect sizes, degrees of freedom and *P* value noted *Give P values as exact values whenever suitable.*
☒	☐	For Bayesian analysis, information on the choice of priors and Markov chain Monte Carlo settings
☒	☐	For hierarchical and complex designs, identification of the appropriate level for tests and full reporting of outcomes
☒	☐	Estimates of effect sizes (e.g. Cohen's *d*, Pearson's *r*), indicating how they were calculated
☐	☒	Clearly defined error bars *State explicitly what error bars represent (e.g. SD, SE, CI)*

Our web collection on statistics for biologists may be useful.

Software and code

Policy information about availability of computer code

Data collection	Cell death was recorded with Incucyte and Cell Titer Glo assays were run on the Mithras LB 940. For RNA seq libraries to be multiplexed in the same run were pooled in equimolar quantities, calculated from Qubit and Bioanalyser fragment analysis. Samples were sequenced on the NextSeq 500 instrument (Illumina, San Diego, US) using a either a 43bp or 81bp paired end run. LC-MS/MS was performed on a Q Exactive Orbitrap Plus interfaced to a NANOSPRAY FLEX ion source and coupled to an Easy-nLC 1000 (Thermo Scientific). Peptides were separated on a 24 cm fused silica emitter, 75 µm diameter, packed in-house with Reprosil-Pur 200 C18-AQ, 2.4 µm resin (Dr. Maisch) using a linear gradient from 5% to 30% Acetonitrile/ 0.1% Formic acid over 10min (for TBK1 AP-MS) or 30 min (for TNFR-SC AP-MS and kinase assay), at a flow rate of 250 nL/min. Precursor ions were measured in a data-dependent mode in the orbitrap analyser at a resolution of 70,000 and a target value of 3e6 ions. The ten most intense ions from each MS1 scan were isolated, fragmented in the HCD cell, and measured in the orbitrap at a resolution of 17,500.
Data analysis	Quantifications were performed with Excel, ImageJ and GraphPad and statistical analysis with GraphPad. Images and figures were processed with Adobe Photoshop and Illustrator CS6, respectively. For RNAseq analysis data were demultiplexed and converted to fastq files using Illumina's bcl2fastq Conversion Software v2.19. Next, the expression of Illumina paired RNA-Seq transcript counts was quantified using kallisto software65 and a GRCh38 transcript model. The data was imported to the R statistical environment and summarised at the gene level (i.e transcript counts summed) using tximport.

Statistical transformations and analysis of differential expression were performed with DESeq271.
Relevant transcripts were illustrated using BioVenn software.

For protein and phosphosite identification raw data were analysed with MaxQuant version 1.5.2.8 where they were searched against the human UniProt database (http://www.uniprot.org/, downloaded 22/10/2015 (for TNFR-SC AP-MS) and 05/10/2017 (for TBK1 AP-MS and kinase assay) using default settings. Label-free quantification in MaxQuant was used to quantify the AP-MS data.

For processing of the TNFR1-SC and TBK1 AP-MS data a protein-protein interaction network was generated in the STRING protein-protein interaction database using known interactions from curated databases and experimentally determined at default settings.

For manuscripts utilizing custom algorithms or software that are central to the research but not yet described in published literature, software must be made available to editors/reviewers upon request. We strongly encourage code deposition in a community repository (e.g. GitHub). See the Nature Research guidelines for submitting code & software for further information.

Data

Policy information about availability of data

All manuscripts must include a data availability statement. This statement should provide the following information, where applicable:

- Accession codes, unique identifiers, or web links for publicly available datasets
- A list of figures that have associated raw data
- A description of any restrictions on data availability

The RNA-Seq dataset generated during the current study are available in the SRA repository and can be accessed by using the following BioProject accession: PRJNA422567 or SRA accession: SRP126844 (https://www.ncbi.nlm.nih.gov/Traces/study/?acc=SRP126844).

The proteomic data has been deposited on the ProteomeXchange Consortium via the PRIDE(ref) partner repository with the dataset identifier PXD008497 (TNFR1-SC analysis), PXD010777 (TBK1 analysis), and PXD008518 (RIPK1 kinase assay).

Field-specific reporting

Please select the best fit for your research. If you are not sure, read the appropriate sections before making your selection.

☒ Life sciences ☐ Behavioural & social sciences ☐ Ecological, evolutionary & environmental sciences

For a reference copy of the document with all sections, see nature.com/authors/policies/ReportingSummary-flat.pdf

Life sciences study design

All studies must disclose on these points even when the disclosure is negative.

Sample size	No statistical method was used to determine the correct sample size. Instead the sample sizes were determined based on our experiences from previous studies using similar methodologies.
Data exclusions	No data was excluded from the study.
Replication	All biological experiments were carried out under clearly defined and standard conditions and were repeated at least twice whenever possible. All replication attempts were successful.
Randomization	Mice were randomly allocated to experimental groups.
Blinding	In vivo experiment was done by a scientist blinded to the treatment schedule. The in vitro experiments were not carried out blinded but most of them were done in parallel by at least two researchers.

Reporting for specific materials, systems and methods

Materials & experimental systems

n/a	Involved in the study
☐	☒ Unique biological materials
☐	☒ Antibodies
☐	☒ Eukaryotic cell lines
☒	☐ Palaeontology
☐	☒ Animals and other organisms
☒	☐ Human research participants

Methods

n/a	Involved in the study
☒	☐ ChIP-seq
☒	☐ Flow cytometry
☒	☐ MRI-based neuroimaging

Unique biological materials

Policy information about availability of materials

Obtaining unique materials: Knockout cell lines were generated using the CRISPR-Cas9 system and are readily available under request upon publication of the study.

Antibodies

Antibodies used: p-TBK1 (Cell Signaling, 5483); TBK (Cell signaling, 3013); p-IKKe (Cell signaling, 8766); IKKe (Cell signaling, 2905); p-IKKa/b (Cell signaling, 2697); RIPK1 (Cell signaling, 3493); p-IkBa (Cell Signaling, 9246); IkBa (Cell signaling, 9242); p-ERK1/2 (Cell signaling, 4370); ERK1/2 (Cell signaling, 4695); p-JNK (Cell signaling, 4671); JNK (Cell signaling, 9258); p-p38 (Cell signaling, 9215); p-RIPK1 S166 (Cell signaling, 65746); murine p-RIPK1 S166 (Cell signaling, 31122); cleaved murine Caspase-8 (Cell signaling, 9429); HOIP (Ubiquigent, 68-0013-100); SHARPIN (Proteintech, 14626-1-AP); RIPK1 (BD, 610459); TNFR-1 (Santa Cruz, SC-8436); GAPDH (Abcam, ab8245); Actin (Sigma, A1978); M1-Ubiquitin (Merck Millipore, MABS199); p38 (Santa Cruz Biotech, sc-728); murine caspase-8 (Enzo Life Sciences, C15); p-MLKL (Abcam, ab187091); murine p-MLKL (Abcam, ab196436); murine RIPK3 (Enzo Life Sciences, ADI-905-242-100); FLAG (Sigma, M2); FADD (Enzo Life Sciences, 1F7); FADD (Santa Cruz, H-181); TANK (R&D Systems; AF4755); AZI2 / NAP1 (abcam, ab192253); Optineurin (abcam, ab151240); IKKγ (Santa Cruz,FL-419; sc-8330); SINTBAD (Cell Signaling, 8605); HOIL-1 (made in house); IKKa (Santa Cruz, B-8; sc-7606); TRAF2 (Enzo Life Sciences, ADI-AAP-422-D); FADD (Santa Cruz Biotech, sc-6036/M-19).
All antibodies used in this study were diluted 1:1000. Only p-IKKe (Cell signaling, 8766) was used 1:500 and Actin (Sigma, A1978) was diluted 1:10000.

Validation: p-TBK1 (Cell Signaling, 5483); validation https://www.cellsignal.com/products/primary-antibodies/phospho-tbk1-nak-ser172-d52c2-xp-rabbit-mab/5483
TBK (Cell signaling, 3013); validation: https://www.cellsignal.com/products/primary-antibodies/phospho-tbk1-nak-ser172-d52c2-xp-rabbit-mab/5483?site-search-type=Products&N=4294956287&Ntt=phospho-tbk1+%28s172%29+%28d52c2%29+xp%C3%82%C2%AE+&fromPage=plp
p-IKKe (Cell signaling, 8766); validation: https://www.cellsignal.com/products/primary-antibodies/phospho-ikke-ser172-d1b7-rabbit-mab/8766
IKKe (Cell signaling, 2905); validation: https://www.cellsignal.com/products/primary-antibodies/ikke-d20g4-rabbit-mab/2905
p-IKKa/b (Cell signaling, 2697); validation: https://www.cellsignal.com/products/primary-antibodies/phospho-ikka-bser176-180-16a6-rabbit-mab/2697
RIPK1 (Cell signaling, 3493); validation: https://www.cellsignal.com/products/primary-antibodies/rip-d94c12-xp-rabbit-mab/3493
p-IkBa (Cell Signaling, 9246); validation: https://www.cellsignal.com/products/primary-antibodies/phospho-ikba-ser32-36-5a5-mouse-mab/9246
IkBa (Cell signaling, 9242); validation: https://www.cellsignal.com/products/primary-antibodies/ikba-antibody/9242
p-ERK1/2 (Cell signaling, 4370); validation: https://www.cellsignal.com/products/primary-antibodies/phospho-p44-42-mapkerk1-2-thr202-tyr204-d13-14-4e-xp-rabbit-mab/4370
ERK1/2 (Cell signaling, 4695); validation: https://www.cellsignal.com/products/primary-antibodies/p44-42-mapk-erk1-2-137f5-rabbit-mab/4695
p-JNK (Cell signaling, 4671); validation: https://www.cellsignal.com/products/primary-antibodies/phospho-sapk-jnk-thr183-tyr185-98f2-rabbit-mab/4671
JNK (Cell signaling, 9258); validation: https://www.cellsignal.com/products/primary-antibodies/jnk2-56g8-rabbit-mab/9258
p-p38 (Cell signaling, 9215); validation: https://www.cellsignal.com/products/primary-antibodies/phospho-p38-mapk-thr180-tyr182-3d7-rabbit-mab/9215
p-RIPK1 S166 (Cell signaling, 65746); validation: https://www.cellsignal.com/products/primary-antibodies/phospho-rip-ser166-d1l3s-rabbit-mab/65746
murine p-RIPK1 S166 (Cell signaling, 31122); validation: https://www.cellsignal.com/products/primary-antibodies/phospho-ripser166-
antibody-rodent-specific/31122
cleaved murine Caspase-8 (Cell signaling, 9429) validation: https://www.cellsignal.com/products/primary-antibodies/cleavedcaspase-
8-asp387-antibody-mouse-specific/9429
HOIP (Ubiquigent, 68-0013-100); validated by using ctr versus HOIP KO cells
SHARPIN (Proteintech, 14626-1-AP); validated by using ctr versus SHARPIN KO cells
RIPK1 (BD, 610459); validation: http://www.bdbiosciences.com/us/applications/research/apoptosis/purified-antibodies/purifiedmouse-
anti-rip-38rip/p/610459
TNFR-1 (Santa Cruz, SC-8436); validation: https://www.scbt.com/scbt/product/tnf-r1-antibody-h-5

GAPDH (Abcam, ab8245); validation: https://www.abcam.com/gapdh-antibody-6c5-loading-control-ab8245.html
Actin (Sigma, A1978); validation: https://www.sigmaaldrich.com/catalog/product/sigma/a1978?lang=en&region=GB&gclid=EAIaIQobChMIml25oIuA3QIVDbTtCh2DJgebEAAYASAAEgJlm_D_BwE
M1-Ubiquitin (Merck Millipore, MABS199); validation: http://www.merckmillipore.com/GB/en/product/Anti-Linear-Ubiquitinclone-1E3-Antibody,MM_NF-MABS199
p38 (Santa Cruz Biotech, sc-728); validation: https://www.scbt.com/scbt/product/p38alpha-antibody-n-20
murine caspase-8 (Enzo Life Sciences, C15); validation by using Caspase-8 KO MEFs versus wt MEFs
p-MLKL (Abcam, ab187091); validation: https://www.abcam.com/mlkl-phospho-s358-antibody-epr9514-ab187091.html
murine p-MLKL (Abcam, ab196436); validation: https://www.abcam.com/mlkl-phospho-s345-antibody-epr95152-ab196436.html
murine RIPK3 (Enzo Life Sciences, ADI-905-242-100); validation: http://www.enzolifesciences.com/ADI-905-242/rip3-polyclonalantibody/
FLAG (Sigma, M2); validation: https://www.sigmaaldrich.com/catalog/product/sigma/f1804?lang=en&region=GB&gclid=EAIaIQobChMIgrjX1I2A3QIVBbXtCh1HrQLgEAAYASAAEgJhUfD_BwE
FADD (Enzo Life Sciences, 1F7); validation: http://www.enzolifesciences.com/ADI-AAM-212/fadd-monoclonal-antibody-1f7/
FADD (Santa Cruz, H-181); validation: https://www.scbt.com/scbt/product/fadd-antibody-h-181
TANK (R&D Systems; AF4755); validation: https://www.rndsystems.com/products/human-mouse-tank-antibody_af4755
AZI2 / NAP1 (abcam, Ab192253); validation: https://www.abcam.com/azi2-antibody-epr14698-c-terminal-ab192253.html
Optineurin (abcam, ab151240); validation: https://www.abcam.com/optineurin-antibody-ab151240.html
IKKγ (Santa Cruz,FL-419; sc-8330); validation: https://www.scbt.com/scbt/product/ikkgamma-antibody-fl-419
SINTBAD (Cell Signaling, 8605); validation: https://www.cellsignal.co.uk/products/primary-antibodies/sintbad-d1a5-rabbitmab/8605
HOIL-1 (Home made; validated by comparing lysates from HOIL-1 KO to control cells)
IKKa (Santa Cruz, B-8; sc-7606); validation: https://www.scbt.com/scbt/product/ikkalpha-antibody-b-8#
TRAF2 (Enzo Life Sciences, ADI-AAP-422-D); validation: http://www.enzolifesciences.com/ADI-AAP-422/traf2-polyclonal-antibody/
FADD (Santa Cruz Biotech, sc-6036/M-19); validation: https://www.scbt.com/scbt/product/fadd-antibody-m-19

Most of the listed antibodies have been used in our laboratory for many years and have been carefully validated using knockout MEFs or more recently via different techniques including siRNA kd, CrispR, TALEN or ZNF approach to achieve knockout cells. Many antibodies were also validated by the provider as stated on their website.

Eukaryotic cell lines

Policy information about cell lines

Cell line source(s)	A549 and HeLa cells were sourced from ATCC, IKKa/b KO MEFs were provided by Matthieu Bertrand, NEMO KO MEFs were provided from Manolis Pasparakis. HOIP KO MEFs were generated in our lab as well as TNF KO MEFs. All other knockout cells presented in this study were generated in our lab using the CRISPR-Cas9 system.
Authentication	Authentication was not performed as none of the cells used have been listed in the commonly misidentified lines.
Mycoplasma contamination	All cell lines were regularly tested for mycoplasma using the MycoAlert™ Mycoplasma Detection Kit (LONZA)
Commonly misidentified lines (See ICLAC register)	No misidentified lines were used in this study

Animals and other organisms

Policy information about studies involving animals; ARRIVE guidelines recommended for reporting animal research

Laboratory animals	Six- to eight-week old female C57BL/6N mice were used in this study
Wild animals	No wild animals were used in this study
Field-collected samples	No field-collected samples were used in this study